國立臺灣大學電機資訊學院生醫電子與資訊學研究所

碩士論文

Graduate Institute of Biomedical Electronics and Bioinformatics
College of Electrical Engineering and Computer Science
National Taiwan University
Master's Thesis

脫附型電噴灑游離法質譜成像探討多系統萎縮症患者腦區的脂質混亂及其與 α-突觸核蛋白聚集的空間關聯研究

Exploring Lipid Disturbances and its Spatial Association with α-Synuclein Aggregation in MSA Patient Brain Regions via Desorption Electrospray Ionization Mass Spectrometry Imaging

張景曜

Ching-Yao Chang

指導教授: 曾宇鳳 博士

Advisor: Yufeng Jane Tseng, Ph.D.

中華民國 112 年 11 月

November 2023

doi:10.6342/NTU202304442

誌謝

從醫學領域跨越到資訊領域，在讀碩士班的這段時間確實不容易，不過一路上也得到來自許多人的協助。首先要感謝本研究中的人腦組織，作為大體老師無私奉獻，提供醫學研究上寶貴的器官樣本，使疾病研究得以更加深入。感謝指導教授曾宇鳳老師的指導，從研究方向的確立到論文架構的細節，曾老師提供了許多建議，我才能更順利地讓論文逐漸趨於完整。感謝台大醫院合作的郭明哲醫師聯絡提供組織樣品，針對整體研究方向提出許多想法，也在學術的路上給予我許多想法及鼓勵。感謝化學系合作徐丞志老師實驗室的興翔學長、宇萱及智翔幫忙操作質譜影像實驗。感謝生醫電資所及台灣大學提供良好的學習環境及充足的研究資源。也要感謝 CMDM 實驗室的夥伴們，包括天爵學長提供許多在實驗上及資料分析上許多實用的建議，又可學姊辛苦協助各實驗室聯絡並且在資料結果呈現上提供不少建議，淯元、岳辰、柏仰等同學們對彼此互相的督促及交換想法，讓我能維持繼續向前的動力。感謝身邊軒羽、瑜倢、怡媗、瑞季、梓維、學文等好友們，在我遇到瓶頸時適時地給予我鼓勵扶持，最後感謝我的父母兄弟們能夠在各方面支持我完成碩士班的研究。

doi:10.6342/NTU202304442

中文摘要

多系統萎縮症是一種罕見的神經退化疾病，因伴隨著 α-突觸核蛋白的異常堆積而被歸類為一種共核蛋白病。過去有許多研究觀察到多系統萎縮症病人血漿及腦脊髓液中的代謝體變化，但因 α-突觸核蛋白堆積導致的代謝體分佈異常仍不清楚。

脫附型電噴灑游離法質譜成像利用軟性離子化技術，幫助辨識並呈現出組織上的分子分佈。我們將脫附型電噴灑游離法質譜成像應用在 12 個受到多系統萎縮症影響的腦區，包含了前額葉皮質、眶額葉皮質、運動皮質、感覺皮質、枕葉皮質、胼胝體、鉤束、視丘、殼核、尾狀核、小腦蚓部、大腦小腦（小腦外側），比較疾病與正常組織的脂質表現及其空間分佈。另外，我們利用免疫組織染色法得到 α-突觸核蛋白堆積之分佈，將質譜影像及組織染色影像進行空間對準來觀察蛋白質堆積及脂質分佈的空間關聯性。

本研究證實了脫附型電噴灑游離法質譜成像應用於多系統萎縮症相關脂質混亂的可應用性，簡化樣本製備程序並且減少游離法對於組織的傷害。我們也發現多系統萎縮症對於不同腦區造成的脂質混亂以及 α-突觸核蛋白與這些脂質分子分佈的空間關聯。

關鍵字：脫附型電噴灑游離法質譜成像、脂質混亂、分子分佈、α-突觸核蛋白、多系統萎縮症

doi:10.6342/NTU202304442

ABSTRACT

Multiple system atrophy (MSA) is a rare neurodegenerative disease categorized as a synucleinopathy characterized by the abnormal accumulation of α-synuclein. Metabolite changes have been observed in MSA patients' biofluids, such as plasma and cerebrospinal fluid. However, understanding the spatial distribution of these metabolites in different brain regions is still limited.

Desorption electrospray ionization mass spectrometry imaging (DESI-MSI) is a soft ionization technique that can identify and visualize the distribution of molecules in tissues. Here, we applied DESI-MSI to 12 different regions of human brain tissues, including the prefrontal cortex, orbitofrontal cortex, motor cortex, sensory cortex, occipital cortex, corpus callosum, uncinate fascicle, thalamus, putamen, caudate, vermis, and cerebrocerebellum, thus covering most of the affected brain regions in MSA patients. We compared the lipid expression of fresh frozen samples and investigated the distribution of the altered lipids. Additionally, we used immunohistochemistry (IHC) staining to visualize the spatial distribution of α-synuclein. We performed image registration of histological images and mass spectrometry images to explore the correlation between the distribution of α-synuclein and the identified lipids.

Our findings demonstrated the utility of DESI-MSI in analyzing MSA-related lipid disturbances in brain tissues with a simple sample preparation process and minimal tissue damage. Moreover, our study provides insight into the spatial distribution of lipids in different brain regions affected by MSA and their correlation with the distribution of α-synuclein.

doi:10.6342/NTU202304442

Keywords: Desorption electrospray ionization mass spectrometry imaging (DESI-MSI), lipid disturbances, molecular distribution, α-synuclein, multiple system atrophy

doi:10.6342/NTU202304442

CONTENTS

doi:10.6342/NTU202304442

doi:10.6342/NTU202304442

doi:10.6342/NTU202304442

LIST OF FIGURES

doi:10.6342/NTU202304442

doi:10.6342/NTU202304442

LIST OF TABLES

doi:10.6342/NTU202304442

GLOSSARY

Cer	Ceramide
CSF	Cerebrospinal Fluid
DESI	Desorption Electrospray Ionization
EPA	Eicosapentaenoic Acid
GalCer	Galactosylceramide
Gb2	Galabiosylceramide
GCI	Glial Cytoplasmic Inclusions
HC	Healthy Control
H&E	Hematoxylin and Eosin
IHC	Immunohistochemistry
LacCer	Lactosylceramide
MSA	Multiple System Atrophy
MSI	Mass Spectrometry Imaging
PA	Phosphatidic Acid
PC	Phosphatidylcholine
PE	Phosphatidylethanolamine
PS	Phosphatidylserine
m/z	Mass-to-charge Ratio
UMAP	Uniform Manifold Approximation and Projection

doi:10.6342/NTU202304442

Chapter 1 Introduction

1.1 Mass Spectrometry Imaging (MSI)

Mass Spectrometry Imaging (MSI) is a technique that utilizes mass spectrometry to identify molecules, such as lipids, proteins, and other metabolites, and clarify their spatial distribution in tissue samples. Although typical mass spectrometry is powerful enough to accurately identify molecules in biological samples, it ionizes and detects them based on the mass-to-charge ratio (m/z). During this process, all the ionized molecules are pooled together, resulting in the loss of spatial information within the sample. MSI provides a solution by setting a certain angle between the ion source and the sample, allowing the detection of ionized molecules to reflect their respective location on the sample. As a result, it can be used to identify the molecules in the sample while simultaneously retaining spatial information. After defining the (x, y) grid on the tissue sample, the mass spectrum of each pixel will be collected until the entire tissue sample is scanned through.[1] Some software can select a specific m/z value, and the distribution of the signal intensities over the tissue sample regarding the specified m/z value can be retrieved. The intensities are presented in the form of a heatmap, allowing for clear visualization of the spatial distribution of the candidate molecules contributing to that m/z value.

Until now, there have been several ionization methods. The most commonly used ionization techniques include secondary ion mass spectrometry (SIMS), matrix-assisted laser desorption ionization (MALDI), and desorption electrospray ionization (DESI).[2] These methods are typically chosen based on the target analytes and their mass range. They exhibit different efficiencies, sensitivities, and spatial resolutions, while the sample preparation procedures vary. SIMS is highly sensitive for analyzing small molecules or elemental ions. Additionally, it provides good spatial resolution on a small scale. All these

doi:10.6342/NTU202304442

advantages come at the cost of its limited mass range for analyzing the molecules. SIMS has also been reported to be more destructive to the tissue due to the nature of ion sputtering on the sample. MALDI allows for a broader range of analytes, detecting everything from small metabolites to multiunit molecules, such as proteins or lipids. The drawbacks include the time-consuming sample preparation step and the potential damage to the tissue sample caused by ultraviolet lasers. DESI, by contrast, is less destructive to the tissue. It is advantageous as it allows for a relatively simple sample preparation step. Moreover, it can detect a mass range from small molecules to polypeptides, sufficient for most metabolomic and proteomic studies. We applied DESI as the ion source of the experiment in the study, as we wanted to preserve the structure of the tissues as much as possible to compare the mass spectrometry images with histological images of the tissues.

1.2 Medical Applications of MSI

MSI is a label-free and on-tissue scanning technique for directly identifying molecules on tissue samples without losing spatial information.[3] It allows the visualization of molecular distribution in the tissues and mapping to other medical image modalities. As a result, it has been widely used in the medical field. Xin Ma *et al*. reviewed some recent studies on cancer metabolomics and lipidomics using MSI and elucidated the correlation between lipid profiles and the progression of various types of cancer.[4] For example, in 2019, Randall *et al.* performed MSI on ten prostate tissue specimens assigned with Gleason Scores (GSs) in different tissue regions to indicate cancer invasiveness. The authors found an overall increase in phosphatidylcholine in tumor regions regardless of GS. Phosphatidic acid, phosphatidylserine, and ceremide-1-phosphate increased in the areas with higher GS, which meant that the distribution of these elevated lipids conformed

doi:10.6342/NTU202304442

to that of the cell malignancy in the cancerous tissues.[5] In 2021, Tu *et al.* applied MSI to six bladder tumors with adjacent normal tissues. The authors found increases in phosphatidylcholine and phosphatidylethanolamine and decreases in sphingomyelin and ceremide in the tumor regions compared to the levels in adjacent normal tissues.[6] In 2023, Aramaki *et al.* performed a lipidomic analysis with DESI-MSI on 12 invasive breast cancer tissues. The authors identified that some lipid species, such as triglyceride, phosphatidylcholine, phosphatidylethanolamine, sphingomyelin, and ceremide species with a higher number of carbon atoms and double bonds, are positively correlated with the malignancy of cancerous tissue by mapping the mass spectrometry images to the histological images.[7] Other studies have also indicated disturbances in small molecules, lipids, or proteins related to various diseases. In 2020, Zhang *et al.* identified lipid abnormalities in diabetic renal proximal tubules using DESI-MSI and found that increased levels of fatty acids, ceramides, phosphatidylethanolamine, phosphatidylglycerol, phosphatidylinositol, and phosphatidylserine indicated the changes in mitochondrial membrane components, as those lipids were mainly localized in the mitochondria-rich tubules.[8] In 2017, Maccarrone *et al.* performed a proteomic analysis using MALDI-MSI on one human brain with multiple sclerosis; evaluated areas included normal white matter, ordinary gray matter, and the lesion. The results were mapped to histological images with immunostaining of the lesions, and they identified thymosin beta-4 as a potential biomarker for multiple sclerosis.[9] In 2016, Hare *et al.* used laser ablation-inductively coupled plasma-mass spectrometry imaging on four brain tissues with Alzheimer's disease to analyze iron distribution in the white and gray matter in the frontal cortex. The authors indicated the neurotoxicity and neurodegeneration caused by iron.[10] These studies provided examples of how different types of metabolites affect the disease pathogenesis and progression. MSI can detect such alterations by visualizing

doi:10.6342/NTU202304442

molecular distribution and mapping to the traditional histological images. In addition to discovering diagnostic biomarkers, MSI is useful in pharmaceutical research. Schulz *et al*. listed several studies that demonstrated the application of MSI in drug distribution, drug metabolism, drug-induced toxicity, and other related fields.[11] For example, Bonnel *et al*. performed MALDI-MSI and quantitative penetration testing for topical medication, roflumilast, tofacitinib, ruxolitinib, and LEO 29102 and screened for the molecules and formulation that had the best penetration ability. Determining the drug concentration and spatial distribution across layers of skin tissue can be used to evaluate whether the concentration in the target lesion is high enough to be effective.[12] Blanc *et al.* used MALDI-MSI to visualize the distribution of tuberculosis drugs, rifampicin, and moxifloxacin and the metabolite changes to assess the drug-mediated response of tuberculosis in rabbit lungs.[13] In 2015, Nilsson *et al*. used MALDI-MSI to visualize the distribution of antibiotic accumulation in the rat kidney. The authors demonstrated the utility of MSI for clarifying the more detailed mechanism for drug-induced renal toxicity.[14] Overall, these studies have elucidated the connection between the molecular distribution acquired by MSI and the other imaging modalities or various medical interventions to provide detailed insight into molecular expression affected by disease progression or the course of treatment.

Nevertheless, changes in metabolite expression can be profoundly affected by proteins in the tissue. Additionally, some diseases etiologies include abnormal protein expression. For instance, most neurodegenerative diseases are known for protein deposition, which can lead to the loss of structure and function of neural cells. While the metabolomic alterations of these diseases are being clarified, it is necessary to understand how protein expression affects the distribution of metabolites. The combination of MSI and tissue staining targeting a specific protein may be a solution to address this objective.

doi:10.6342/NTU202304442

1.3 Multiple System Atrophy (MSA)

Multiple System Atrophy (MSA) is a rare neurodegenerative disease that may affect the autonomic, pyramidal, and cerebellar systems. Typically, MSA is divided into Parkinsonian type (MSA-P) and cerebellar type (MSA-C) based on the symptoms observed at diagnosis and the region of brain impairment. The symptoms of MSA-P, such as limb stiffness and hypokinesia, are similar to those of Parkinson's disease. In contrast, MSA-C symptoms include an unsteady gait, loss of balance, and dysarthria. Moreover, patients with MSA may experience common symptoms due to autonomic impairment, such as postural hypotension, urinary and bowel dysfunction, sleep disorders, and sexual dysfunction.[15]

Wenning *et al.* introduced the criteria for the diagnosis of MSA.[16] Possible prodromal MSA is confirmed with at least one nonmotor feature (REM sleep behavior disorder, neurogenic orthostatic hypertension, or urogenital failure) and one motor feature (subtle parkinsonian or cerebellar signs). Clinically probable MSA requires at least two of the following: autonomic dysfunction, parkinsonism, and cerebellar syndrome with at least one supportive clinical feature. Clinically established MSA requires autonomic dysfunction plus at least one symptom of poor-L-DOPA responsive Parkinsonism or cerebellar syndrome with at least two supportive clinical features. Neuropathologically established MSA requires finding widespread α-synuclein inclusion bodies in glial cells in neural tissue and confirming striatonigral or olivopontocerebellar atrophy on brain autopsy.

α-Synuclein is a well-known protein biomarker for MSA, and its accumulation directly causes neuroinflammation and neurodegeneration, resulting in pathogenesis. Normally, α-synuclein is a protein that regulates synaptic activity in neural cells. It can

doi:10.6342/NTU202304442

control the release of calcium ions, hence increasing ATP-inducing exocytosis. In addition, it enhances vesicle priming and the fusion of exocytotic fusion pores. Overall, α-synuclein plays several roles in regulating synaptic vesicle trafficking and thus affects downstream neurotransmitter release. Structurally, the α-helix motifs in α-synuclein are similar to those of the lipid-binding proteins[16], and the phospholipids in the cell membrane may trigger a conformational change in α-synuclein and initiate the aggregation process.[18] Typically, oligomeric α-synuclein aggregates can be cleared through lysosomal degradation.[19] Once α-synuclein aggregation is enhanced or the clearing procedure is somehow blocked, the accumulation of α-synuclein eventually occurs. Hence, we believe that the accumulation of α-synuclein may correlate with the distribution of some lipids. The abnormal accumulation of α-synuclein characterizes some neurodegenerative diseases, and they are categorized as synucleinopathies, including Parkinson's disease (PD), dementia with Lewy bodies (DLB), and MSA[20] In MSA, one of the most significant pathological features is the presence of α-synuclein-positive glial cytoplasmic inclusions (GCIs) in oligodendrocytes. Although generally widespread, the GCI can show slightly different distributions in different subtypes of MSA.

doi:10.6342/NTU202304442

1.4 Known Metabolite Alterations in MSA patients in Previous Works

1.4.1 Lipids

Some lipids have been proven to be alter in plasma, CSF, and some regions of postmortem brain tissues from patients with MSA. In 2008, Phil Hyu Lee *et al*. conducted a GC/MS experiment on CSF samples from 6 MSA patients and found an elevated level of EPA in CSF. This might explain the compensatory response of EPA to inhibit apoptosis and neuroinflammation during neurodegeneration.[21] In 2019, Mori A *et al*. perfromed a metabolome analysis of plasma samples from 16 MSA patients and 20 healthy controls using LC-TOFMS. The authors found increased levels of several saturated and unsaturated fatty acid species, such as FA(14:0), FA(14:1), and FA(18:0), and decreased levels of lysophosphatidylcholine, LysoPC(16:0), confirming the diagnostic value of each lipid biomarker for MSA. The findings also indicated abnormal lipid metabolism caused by MSA.[22] Later in 2022, Hideki Oizumi *et al*. analyzed plasma from 13 MSA patients and six controls using LC/MS-MS and found an elevated levels of lactosylceramide d18:1 and monohexylceramide d18:1 and a decreased levels of sphingosine-1-phosphate d16:1 and sphingosine-1-phosphate d18:1. The results were consistent with the current understanding that elevated levels of cerebroside species could induce neuroinflammation and cause neurodegeneration.[23] Previous studies also indicated that the abnormal accumulation of α-synuclein downregulates the activity of sphingosine kinase which synthesizes sphingosine-1-phosphate and results in the decrease level of sphingosine-1-phosphate and elevation of ceramide, the material of S1P synthesis, in MSA patients.[24] Although these studies have identified several potential lipid biomarkers and their effects on disease progression, the expression of these lipids in the tissue can differ from those

doi:10.6342/NTU202304442

in CSF and plasma.

In 2014, Don *et al*. performed a lipid assay using LC-MS/MS on lipid extracts of white matter under the motor cortex from 8 MSA patients and 10 controls, and the presence of α-synuclein-positive GCIs in the MSA group was confirmed. The authors identified a decreased levels of sphingomyelin, galactosylceramide, and sulfatide species.[25] Similar experiments were conducted on lipid extracts of the amygdala from 8 MSA patients and 10 controls in the work of Fu *et al*. in 2022, indicating that the accumulation of α-synuclein might be correlated with an increased level of phosphatidylcholine, phosphatidylethanolamine, phosphatidylserine, and sphingomyelin species.[26] These studies demonstrated altered lipid expression in tissue and confirmed their correlation with α-synuclein by ensuring its expression and accumulation. However, understanding the spatial distribution and the correlation between proteins and lipid metabolites is still limited. Table 1.1 summarizes the above research findings on plasma, CSF, and brain tissues from patients with MSA as well as the lipid changes observed, sample types evaluated, and analysis methodologies used in the studies. The abnormal expression of fatty acids, phospholipids, and sphingolipids are three main types of lipid classes characterized by these studies. Unsaturated fatty acids, especially n-3 and n-6, have inflammation-regulating activity.[27][28] Phospholipids and sphingolipids are responsible for signal transduction in the neural system.[29][30] The imbalance of n-3 and n-6 fatty acids can reflect the inflammatory status of tissues, while the abnormal expression of phospholipids and sphingolipids can affect brain development and function. These lipid changes may explain the clinical manifestations of MSA, such as neuroinflammation or neuronal loss.

doi:10.6342/NTU202304442

Table 1.1 Altered lipid levels found in human samples from previous studies related to multiple system atrophy

Sample	Lipid & Alteration	Analysis	Reference
CSF	Increase: EPA	GC-MS	[21]
Plasma	Increase: FA(14:0), FA(14:1), FA(18:0) Decrease: LPC(16:0)	LC-TOFMS	[22]
Plasma	Decrease: S1P(d16:1), S1P(d18:1) Increase: MonCer(d18:1), LacCer(d18:1)	LC-MS/MS	[23]
Motor Cortex	Decrease: SM, sulfatide, GalCer	LC-MS/MS	[25]
Amygdala	Increase: PC, PE, PS, SM	LC-MS	[26]

CSF: cerebrospinal fluid; FA: fatty acid; LPC: lysophosphatidylcholine; S1P: sphingosine-1-phosphate; MonCer: monohexylceramide; LacCer: lactosylceramide; EPA: eicosapentaenoic acid; SM: sphingomyelin, GalCer: galactosylceramide; PC: phosphatidylcholine; PE: phosphatidylethanolamine; PS: phosphatidylserine

1.4.2 Neurotransmitters

Some MSA patients may suffer from parkinsonism due to the loss of dopaminergic neurons.[31] Dopamine is a catecholamine compound mostly synthesized in the brain and kidneys. It is a neurotransmitter in the brain responsible for reward and motivation mechanisms.[32] Other than dopamine, related metabolites involved in the dopamine metabolism pathway have been reported to show significant alterations, mostly decreases, in the CSF of patients with MSA compared to that of controls. These metabolites include DOPA (3,4-dihydroxyphenylalanine), DOPAC (3,4-dihydroxyphenylacetic acid), DHPG (3,5-dihydroxyphenylglycol)[33], HVA (homovanillic acid), and MHPG (3-methoxy-4-hydroxyphenylglycol).[34]

doi:10.6342/NTU202304442

1.4.3 Other Metabolites

Vitamins are a group of organic compounds that play important roles in regulating cell growth and metabolism. In a case-control study by Chen, *et al.*, they found significantly increased level of serum vitamin A and decreased levels of serum vitamin B9 and C in MSA patients compared to the healthy control, indicating dysregulation of vitamin homeostasis in MSA patients. They also found a potential diagnostic value of the combination of these three vitamin levels in the patient serum.[35]

Polyamines are important regulators of cell growth and programmed cell death.[36] In a study by Paik, *et al.*, certain polyamines were associated with Parkinson's disease and MSA. Decreased levels of N1-acetylputrescine, N1-acetylcadaverine, and N1-acetylspermidine, and increased levels of cadaverine and N8-acetylspermidine were noted in the CSF of patients with MSA.[37]

Nitric oxide (NO) has been discovered to exhibit neurotransmission activity. Kuiper *et al.* demonstrated that the levels of citrulline, a material for nitric oxide synthesis, and nitrate, a product of NO degradation, in the CSF are significantly elevated and decreased, respectively.[38][39] Coenzyme Q10 participates in numerous biochemical pathways. It has been found that the concentration of coenzyme Q10 in the CSF is reduced in MSA patients.[40]

doi:10.6342/NTU202304442

1.5 Aims

This study aimed to discover lipid alterations in different brain regions caused by MSA. Moreover, we wanted to clarify the correlation between the spatial distribution of a well-known protein biomarker, α-synuclein, and that of the lipids. As MSA may affect different brain regions and account for various clinical presentations, we used DESI-MSI to quantify the alteration of lipids and uncover the underlying mechanism of these clinical presentations. By utilizing the spatial information provided by MSI, we further mapped the mass spectrometry images to immunohistochemical images targeting α-synuclein to confirm the possible interaction between α-synuclein and the related lipids and to gain detailed insight into how these lipids affected different brain regions. Overall, this study aimed to investigate how abnormal protein and lipid expression play roles in the disease progression of MSA.

doi:10.6342/NTU202304442

Chapter 2 Materials and Methods

2.1 Sample Preparation

We collected the postmortem brains from one MSA patient and one person who served as a healthy control (HC) human; the patient with neuropathologically established MSA was diagnosed by the Department of Pathology, National Taiwan University Hospital. Cryosectioning was performed on 12 brain regions, including the prefrontal cortex, orbitofrontal cortex, motor cortex, sensory cortex, occipital cortex, corpus callosum, uncinate fascicles, thalamus, putamen, caudate, vermis, and cerebrocerebellum (lateral hemisphere of the cerebellum), with a Leica CM1950 cryostat. All sections were cut into three 12-μm-thick slices. Two are used for mass spectrometry imaging experiments for metabolite identification; one is for immunohistochemistry (IHC) staining targeting α-synuclein. After sectioning, all samples were stored in a -80℃ ultra-low-temperature freezer.[41]

2.2 DESI-MSI and Histological Staining

The ion source of DESI was in tandem with Orbitrap Elite for mass spectrometry imaging. Table 2.1 shows the instrument settings for the experiment in negative ion mode. The same sample slides underwent hematoxylin and eosin (H&E) staining for image registration between mass spectrometry and histological images.

IHC staining was performed using the recombinant anti-α-synuclein (phospho S129) antibody from Abcam, Inc. by Toson Technology Co., Ltd. As the aggregation particle of α-synuclein is the size of a micrometer scale, the accumulation level cannot be observed in the visual field of the whole tissue. We used Motic DSAssistant to check the

doi:10.6342/NTU202304442

morphology of the aggregation particles in a 10x magnifying visual field. We defined a 500 μm*500 μm grid on the tissue and counted the amount of the α-synuclein aggregation particles in each grid using ImageJ.[42] For counting the aggregation particles, the images of each grid were converted to 8-bit color, and the color threshold was set from 0 to 50 to retain the most intensive aggregation particles. The particles whose area was under ten pixel-squares were not further evaluated to avoid false discovery, and the particle analyzing module counted the remaining particles. We presented the level of aggregation in a heatmap form to visualize the level of α-synuclein accumulation over slides with the whole tissue samples.

Table 2.1 Instrument settings for the negative ion mode of the mass spectrometry imaging experiment

	Parameter settings for the mass spectrometry imaging experiment
Ion mode	Negative
Solvent	Dimethylformamide / Acetonitrile (1:1)
Flow rate	2 uL/min
Gas pressure	170 psi
Spatial resolution	200 μm
Spray Voltage	-3.5 kV
Capillary temperature	320°C
Mass range	m/z 150-1000
Resolution	60,000

2.3 Image Registration

To determine the spatial correlation between α-synuclein and lipid distribution, every pixel in mass spectrometry and histological images with α-synuclein staining must be well aligned.[52] Image registration is essential in incorporating the complex spatial information of tissues acquired by different methodologies. By integrating with

doi:10.6342/NTU202304442

histological images, we could visualize the spatial relationship between the protein and lipids.

Lin *et al.* proposed an accurate image registration workflow to reduce subjectivity.[53] First, Datacube Explorer was used to manually draw masks for the region of interest (ROI).[54] Total ion count (TIC) normalization and peak picking were then performed using the Python package "pyimzml" (version 1.1.0). Hyperspectral visualization was carried out using uniform manifold approximation and projection (UMAP) as an intensity-based method to reduce the dimensions corresponding to all the detected peaks. The parameter settings for UMAP were as follows: n_components: 3, random_state: 112. The resulting images showed spectral similarity among all the pixels within the selected ROI. On the other hand, the contours of the histological images were detected using the OpenCV library (version 4.7.0). Afterward, a similarity transform method produced an affine transformation matrix to transform the contour of histological images to fit the size and shape of mass spectrometry images using the Python package ITKElastix (version 0.16.0).[55] The resulting binary masks, whose pixel values were 0 in the background area and 1 in the tissue area, were first used to filter out the background signal in the mass spectrometry images and served as the references for resizing the histological images. Afterward, the MS images can be mapped to histological images with a more subjective pixel alignment.

2.4 Peak Annotation and Statistical Analysis

After the MSI experiment, peak annotation was performed to identify candidate metabolites corresponding to each detected mass signal. Peak annotation was performed on the METASPACE platform[43] against the Human Metabolome Database (HMDB,

doi:10.6342/NTU202304442

version 4) and manually validated against HMDB version 5.[44] METASPACE introduced an FDR-controlled annotation algorithm for spatial metabolomics based on a metabolite-signal match (MSM) score and a target-decoy FDR-estimation strategy to avoid false positives produced by traditional methods.[45] The MSM score was calculated based on three indexes: the measure of spatial chaos (ρ_{chaos}), spectral isotope measure ($\rho_{spatial}$), and spatial isotope measure ($\rho_{spectral}$). The measure of spatial chaos defines how well-structured an ion image corresponding to a certain m/z value is.[46] The spectral isotope measure represents the spectral similarity between the isotopic images, and the spatial isotope measure calculates the closeness of the intensities between theoretical and observed isotopic images. The MSM score is the product of all three indexes and serves as the quantification of the possibility that the signal truly exists, as shown in Equation 2.1.

Equation 2.1

$$MSM = \rho_{chaos} * \rho_{spatial} * \rho_{spectral}$$

In addition, a target-decoy approach[47] was applied to calculate the MSM cutoff for the specified FDR. Decoy data are prepared with the same chemical formulas as the targets but with nearly improbable adducts, such as Ag^+, Ni^+, etc. As in Equation 2.2, FDR is calculated as the decoy false positives (FP_D) divided by the sum of the target positives (TP_T) and the target false positives (FP_T). The METASPACE platform allows users to specify an FDR value to choose the MSM cutoff. In this study, we dropped the annotation with FDR > 10% to reduce false positives while maintaining the metabolite annotation amount as much as possible.

Equation 2.2

$$FDR\ estimate = \frac{FP_D}{TP_T + FP_T}$$

doi:10.6342/NTU202304442

The following statistical analysis was conducted on the MetaboAnalyst 5.0 platform to find differentially expressed metabolites between the MSA and control groups.[48] The missing values were imputed by K-nearest neighbor (KNN)-based missing value estimation.[49] Data normalization was followed by autoscaling, in which the data were mean-centered and divided by the standard deviation of each feature. The Mann-Whitney U test detected differences in peak intensities between the MSA and HC groups. Benjamini-Hochberg correction, an FDR-based significance adjustment, was used to correct the strictness when multiple difference tests were performed simultaneously.

2.5 Pathway Analysis

To recognize the possible alteration of biological functions caused by MSA, the pathway analysis was performed to characterize which biochemical pathways were most affected by the disease. The input compound list for pathway analysis included candidate molecules corresponding to the m/z signals with significant differences between the two groups. The KEGG pathway library of *Homo sapiens* served as the reference metabolome.[50]

Regarding lipid molecules, the KEGG pathway only contains information on lipid classes. However, there can be various lipid species within one lipid class. The related pathway information was downloaded from the PubChem pathway database in JSON format to ensure that the detected lipid species can be found in the human metabolic pathway.[51] MetaboAnalyst 5.0 provides a useful module for transferring molecular IDs among databases such as HMDB, PubChem, and METLIN. After transferring the HMDB ID to PubChem Compound ID (CID), we checked whether the detected lipids were previously found to be involved in these pathways based on their PubChem CID and the

doi:10.6342/NTU202304442

number of annotated pathways related to the lipid species that belong to a certain lipid class.

2.6 Dimensionality Reduction and Clustering Analysis

While different lipids can exert varying distributions on the tissue, there can be certain spectral patterns that show biochemical relevance in different regions of the tissue. Clustering analysis has been widely used in MSI data to extract metabolomic patterns in different regions of tissues.[56] As the MSI data contain multiple dimensionalities regarding all the detected signals of m/z values, dimensionality reduction is needed to project all signals into a 2D plane with one additional RGB color space. First, all peaks were grouped by UMAP, and then K-mean clustering was applied for nonhierarchical clustering. The silhouette coefficient defines the performance of the clustering result with the number of clusters, k. [57] The calculation of the silhouette coefficient is as follows:

Equation 2.3

$$a(i) = \frac{1}{|C_I - 1|} \sum_{j \in C_I, i \neq j} d(i,j)$$

Equation 2.4

$$b(i) = \min_{J \neq I} \frac{1}{|C_J|} \sum_{j \in C_J} d(i,j)$$

Equation 2.5

$$s(i) = \begin{cases} 1 - \dfrac{a(i)}{b(i)}, & if a(i) < b(i) \\ 0, & if\ a(i) = b(i), \\ \dfrac{b(i)}{a(i)} - 1, & if\ a(i) > b(i) \end{cases}$$

$$SC = \max_k \tilde{s}(q)$$

In Equation 2.3, d(i, j) is the distance of the data i and j in the same cluster, and C_I is

doi:10.6342/NTU202304442

the number of the data points in cluster C. a(i) is calculated as the mean distance of data i to all other data j in the same cluster C. The divisor is C_I-1 because the distance of one data point to itself is not considered. In Equation 2.4, b(i) is calculated as the minimal mean distance of data i to all other data j that do not belong to the same cluster. A silhouette coefficient is defined in Equation 2.5, where a s(i) value closer to 1 represents a shorter distance of data i to the other data in the same cluster and a larger distance to those in the other clusters, suggesting an appropriate classification. A silhouette coefficient, SC, is the maximum of the mean of s(i), represented as $\tilde{s}(q)$, throughout the entire dataset q. Therefore, a silhouette coefficient closer to 1 means better clustering performance.

In this study, k was set between the values of two and nine, and the number of clusters with the highest silhouette coefficient (Python package, scikit-learn v1.2.2) was chosen as the final number of groups for the samples. The clustering results were then mapped to the IHC staining results of α-synuclein to visualize the correlation between the identified lipid changes and the accumulation of α-synuclein.

doi:10.6342/NTU202304442

Chapter 3 Results

3.1 Metabolite Annotation and Statistical Analysis

After the DESI-MSI experiment, all the detected peaks were annotated against HMDB using the m/z values. The results revealed 283 annotations with unique m/z values in 12 brain regions of the two groups. After data filtering, 251 annotations remained, and most were associated with lipids. As the metabolite annotation of MSI was merely based on the exact mass of the molecules, one m/z value can be referred to as multiple candidate molecules. We manually filtered out the exogenous molecules labeled in HMDB and kept the candidates that take part in the biochemical pathway in the human body. The remaining candidates were considered tentative molecules of the m/z values, and most of them belonged to the superclass of lipids and lipid-like molecules classified by HMDB. The tentative lipid classes of the annotated m/z values are as follows: fatty acid (FA), diacylglycerol (DG), phosphatidic acid (PA), phosphatidylcholine (PC), phosphatidylethanolamine (PE), phosphatidylserine (PS), phosphatidylglycerol (PG), lysophosphatidylcholine (LPC), lysophosphatidylethanolamine (LPE), cardiolipin (CL), ceramide (Cer), sphingomyelin (SM), glucosylceramide (GluCer), galactosylceramide (GalCer), lactosylceramide (LacCer), galabiosylceramide (Gb2), and sulfatide.

Statistical results uncovered 20 m/z values whose tentative molecules belonged to lipids with significant changes in MSA groups. Table 3.1 shows the p value and the adjusted p value (by Benjamini-Holchberg correction) of these m/z values, along with the tentative lipid class. However, the 12 tissue samples in the two groups belonged to different brain regions, and they executed various types of physiological tasks in the human body, so the expression of lipids among the 12 brain regions might vary. Figure 3.1 demonstrates these differentially expressed lipids' different trends and levels across

doi:10.6342/NTU202304442

the 12 brain regions.

Table 3.1 Statistical results of lipid expression in the MSA and HC groups. As we wanted to discover as many disease-related lipids as possible, the α value for hypothesis testing was set to 0.05.

m/z	Lipid	P value	Adjusted p value
301.22	EPA	0.00097656	0.01416008
760.51	PS	0.0048828	0.01416008
810.53	PS	0.0048828	0.01416008
478.29	LPE	0.0048828	0.01416008
886.63	Gb2, LacCer	0.0048828	0.01416008
922.65	PS	0.0048828	0.01416008
331.26	AdA	0.0068359	0.01416008
772.53	PE	0.0068359	0.01416008
786.53	PS	0.0068359	0.01416008
644.50	Cer	0.0068359	0.01416008
701.61	DG	0.0068359	0.01416008
804.53	Sulfatide	0.012207	0.02082371
866.59	PS	0.012207	0.02082371
283.26	STA	0.016113	0.02336385
945.51	CL	0.016113	0.02336385
816.58	PS	0.016113	0.02336385
687.51	SM	0.026855	0.02995365
742.54	PC, PE	0.026855	0.02995365
728.56	PC, PE	0.026855	0.02995365
835.62	PA	0.026855	0.02995365

EPA: eicosapentaenoic acid; PS: phosphatidylserine; LPE: lysophosphatidylethanolamine; Gb2: galabiosylceramide; LacCer: lactosylceramide; AdA: adrenic acid; PE: phosphatidylethanolamine; Cer: ceramide; DG: diacylglycerol; STA: stearic acid; CL: cardiolipin; SM: sphingomyelin; PC: phosphatidylcholine; PA: phosphatidic acid

doi:10.6342/NTU202304442

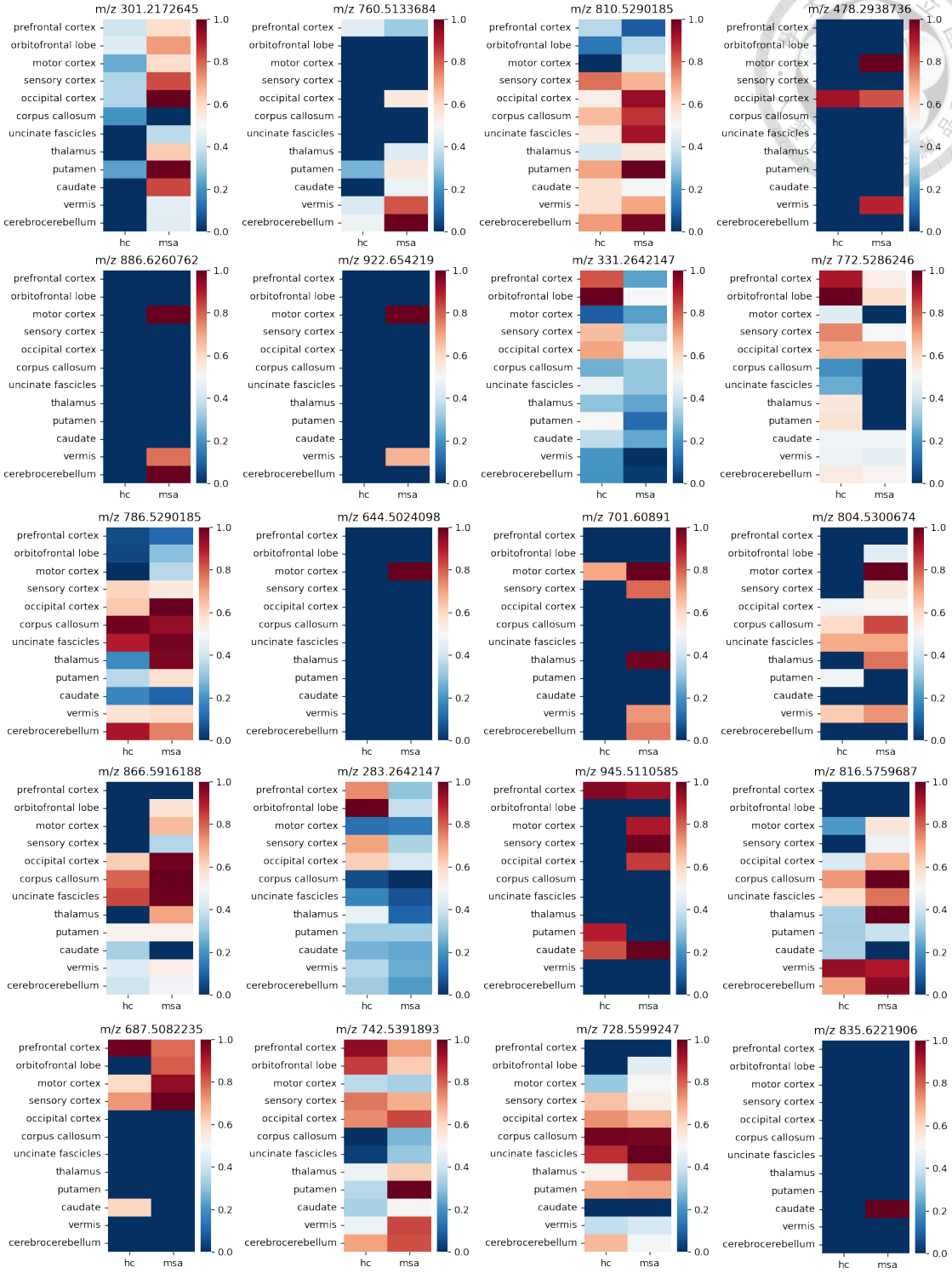

Figure 3.1 The different levels of the differentially expressed lipids in the 12 brain regions. The values are the normalized average intensity of the corresponding m/z signal detected in the tissue samples.

doi:10.6342/NTU202304442

3.2 Related Pathways and Regional Differences

We then looked into the metabolic pathways mainly affected by the MSA and control groups. The molecule list for pathway analysis included the candidate molecules with significant differences in peak intensities, as listed in Table 3.1. The summary and the detailed results of pathway analysis, annotated against the KEGG pathway, are shown in Figure 3.2 and Table 3.2, respectively. The pathway impact is the centrality of the detected metabolites in the pathway. A higher effect indicates a higher centrality, which means that the differentially expressed metabolites can have a higher impact on the overall pathway.

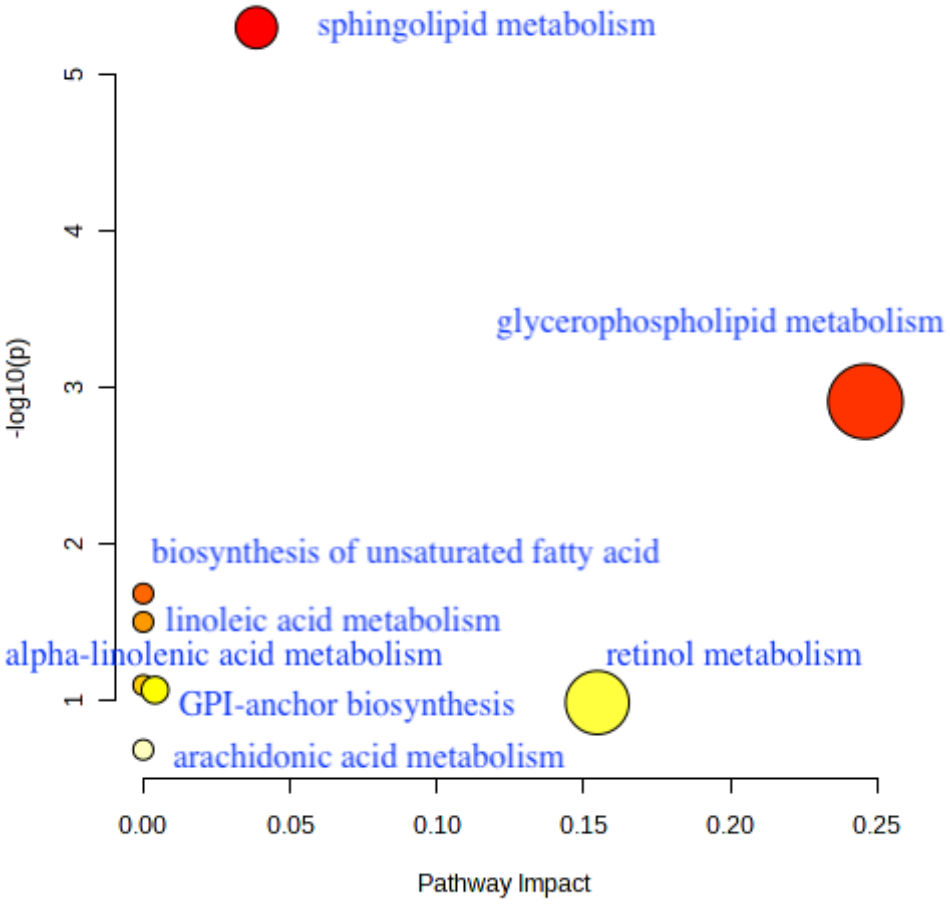

Figure 3.2 Pathway analysis overview.

doi:10.6342/NTU202304442

Table 3.2 The pathway analysis result corresponds to the detected lipids with significant changes between the MSA and HC groups. The 'Total' column represents the number of known molecules participating in the metabolic pathway. The 'Hit' column is the matched lipids in the input molecule list.

Pathway	Total	Hits	Raw p	Log10(p)	FDR	Impact
Sphingolipid metabolism	21	4	4.98E-6	5.3032	0.00041792	0.03854
Glycerophospholipid metabolism	36	3	0.0012358	2.9081	0.051902	0.24596
Biosynthesis of unsaturated fatty acids	36	2	0.020999	1.6778	0.58798	0
Linoleic acid metabolism	5	1	0.031885	1.4964	0.66959	0
alpha-Linolenic acid metabolism	13	1	0.081002	1.0915	1	0
Glycosylphosphatidyl-inositol (GPI)-anchor biosynthesis	14	1	0.086981	1.0606	1	0.00399
Retinol metabolism	17	1	0.10471	0.98002	1	0.15464
Arachidonic acid metabolism	36	1	0.20998	0.67783	1	0

For some lipids, the KEGG pathway only contains the information at the class level, while the PubChem pathway database contains more specific pathway information for lipid molecules down to the species level. This ensures that lipid species with a certain number of carbon atoms or other chemical modifications can be found in the human metabolic pathway. The related pathway information for the list above of molecules was downloaded from the PubChem pathway database, and those with a taxonomy other than *Homo sapiens* were excluded.

A total of 325 pathways were related to the detected lipids. Two hundred thirty-two were related to the de novo biosynthesis of triacylglycerol species. However, Table 3.2 did not show any related pathway, indicating that there might be little difference in the expression of triacylglycerol synthesis between the two groups. Among the three most

doi:10.6342/NTU202304442

affected pathways in Table 3.2, sphingolipid metabolism, glycerophospholipid metabolism, and biosynthesis of unsaturated fatty acids, we detected 17, 87, and 11 lipids, respectively. Overall, the results suggested that these three pathways (metabolism of sphingolipid, glycerophospholipid, and unsaturated fatty acids) could be affected by MSA.

For the detected lipids belonging to the three pathways, we calculated the natural logarithm of the relative fold changes (ln-fold changes) of their averaged intensity in each tissue sample. Figure 3.5 shows each lipid's ln-fold change in the 12 brain regions as clustered heatmaps for the pathways of sphingolipid metabolism, glycerophospholipid metabolism, and biosynthesis of unsaturated fatty acids. To reduce the false discovery, an absolute ln-fold change > 1.5 value was considered to indicate differential expression between the two groups. Since the clustered map of glycerophospholipid shows little consistency among all species across brain regions, we further investigated the ln-fold change in each lipid class that belongs to glycerophospholipid and found a specific pattern of alteration of some phosphatidylserine species, as shown in Figure 3.4(b). These figures also demonstrate the different trends and levels of alteration in lipid expression across other brain regions.

doi:10.6342/NTU202304442

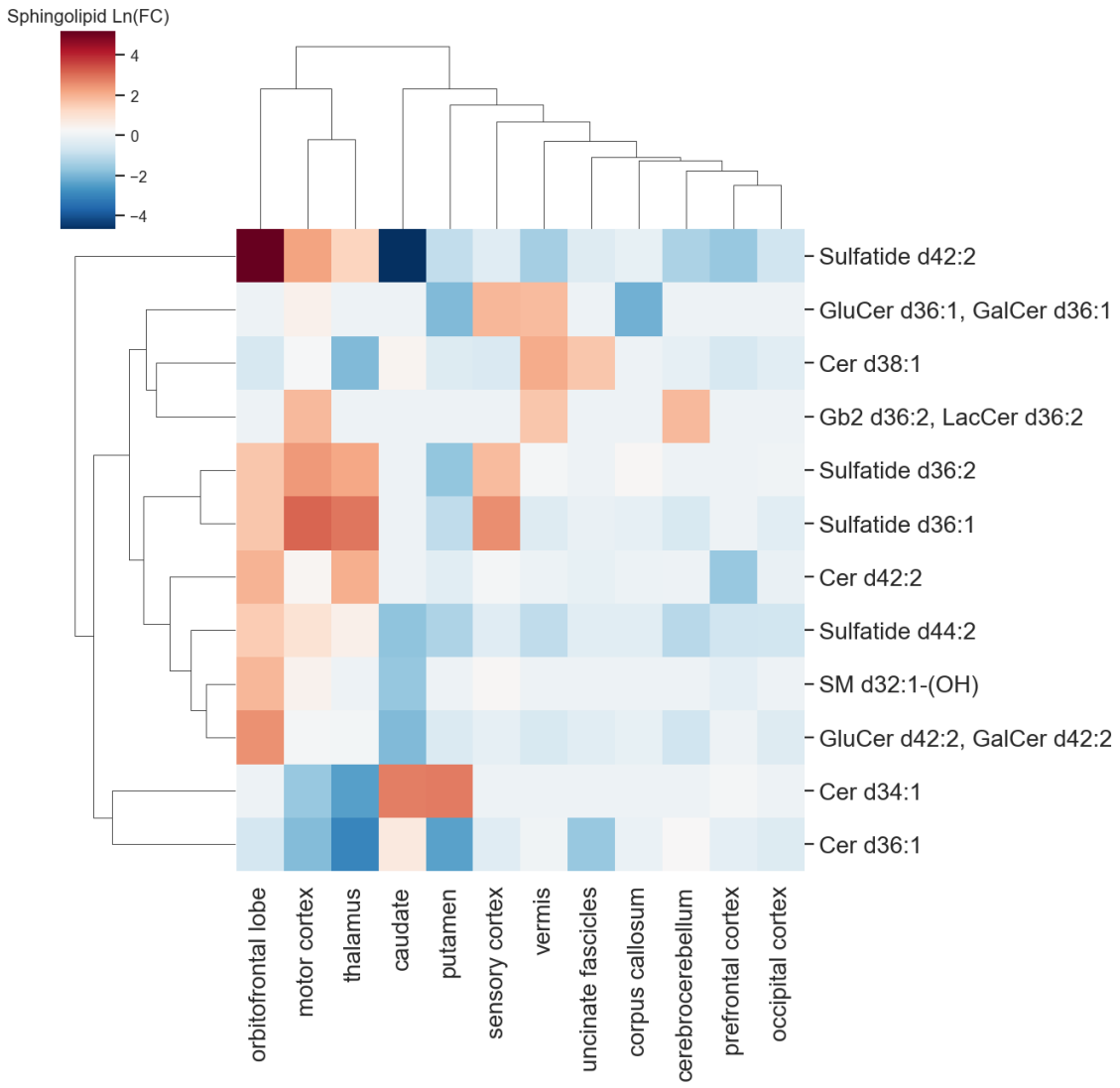

Figure 3.3 The ln-fold change of the averaged intensity of sphingolipid on the 12 brain regions. The x-axis represents the 12 brain regions, while the y-axis represents the lipid names.

doi:10.6342/NTU202304442

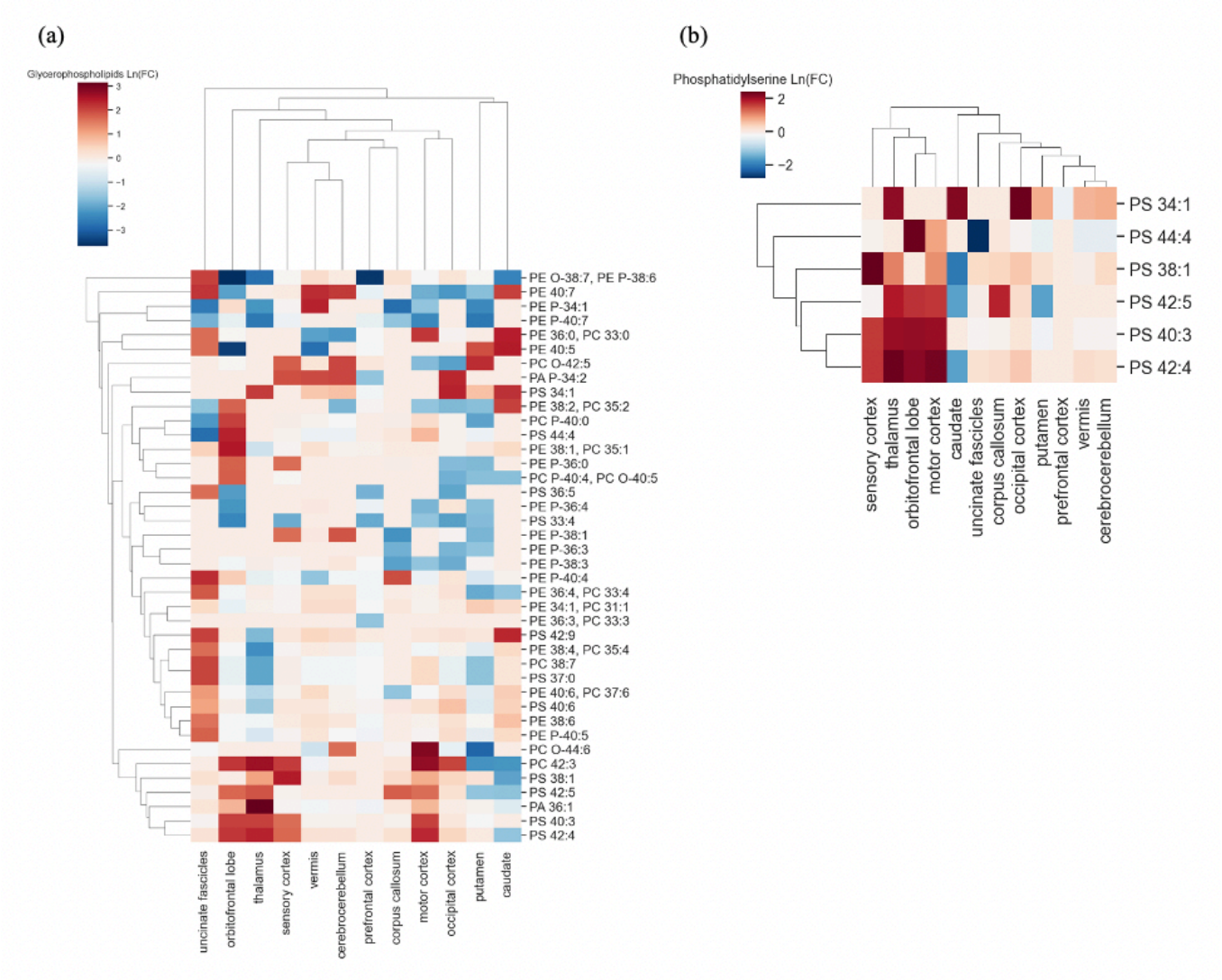

Figure 3.4 The ln-fold change of the averaged intensity of (a) phospholipid and (b) phosphatidylserine on the 12 brain regions. The x-axis represents the 12 brain regions, while the y-axis represents the lipid names.

doi:10.6342/NTU202304442

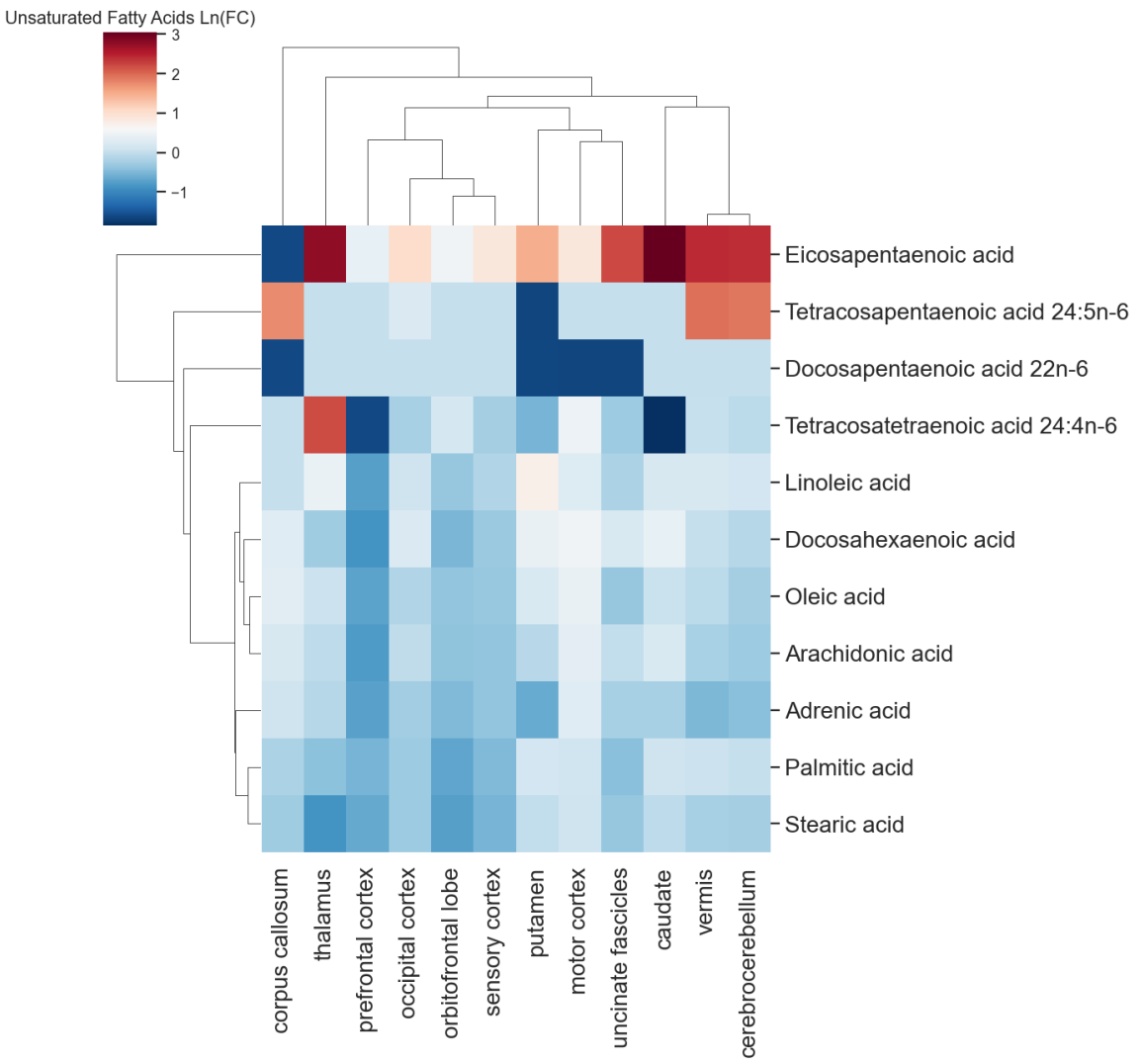

Figure 3.5 The ln-fold change of the averaged intensity of unsaturated fatty acid on the 12 brain regions. The x-axis represents the 12 brain regions, while the y-axis represents the lipid names.

doi:10.6342/NTU202304442

3.3 Clustering Analysis and The Correlation with α-Synuclein Distribution

3.3.1 Clustering

The clustering analysis aimed to find the spectral patterns and classify them into different segments based on those patterns. UMAP and K-means clustering were performed to reduce the dimensionality of mass spectrometry data, visualize the spectral patterns of all detected signals, and group all pixels into a specified number of clusters, k. The number of clusters was optimized by calculating the silhouette coefficient. Figure 3.6 shows the plots of the silhouette coefficient to validate the clustering results and determine the number of clusters for the 12 brain regions in the MSA group. Based on the silhouette evaluation, the number of clusters that yielded the highest silhouette coefficient was selected for each brain region: three for the prefrontal cortex; four for the motor cortex, uncinate fascicles, putamen, and caudate; five for the vermis; six for the occipital cortex and thalamus; seven for the sensory cortex; eight for the orbitofrontal cortex and cerebrocerebellum; and nine for the corpus callosum. The clustering results of the 12 samples from the MSA group are shown in Figure 3.7.

doi:10.6342/NTU202304442

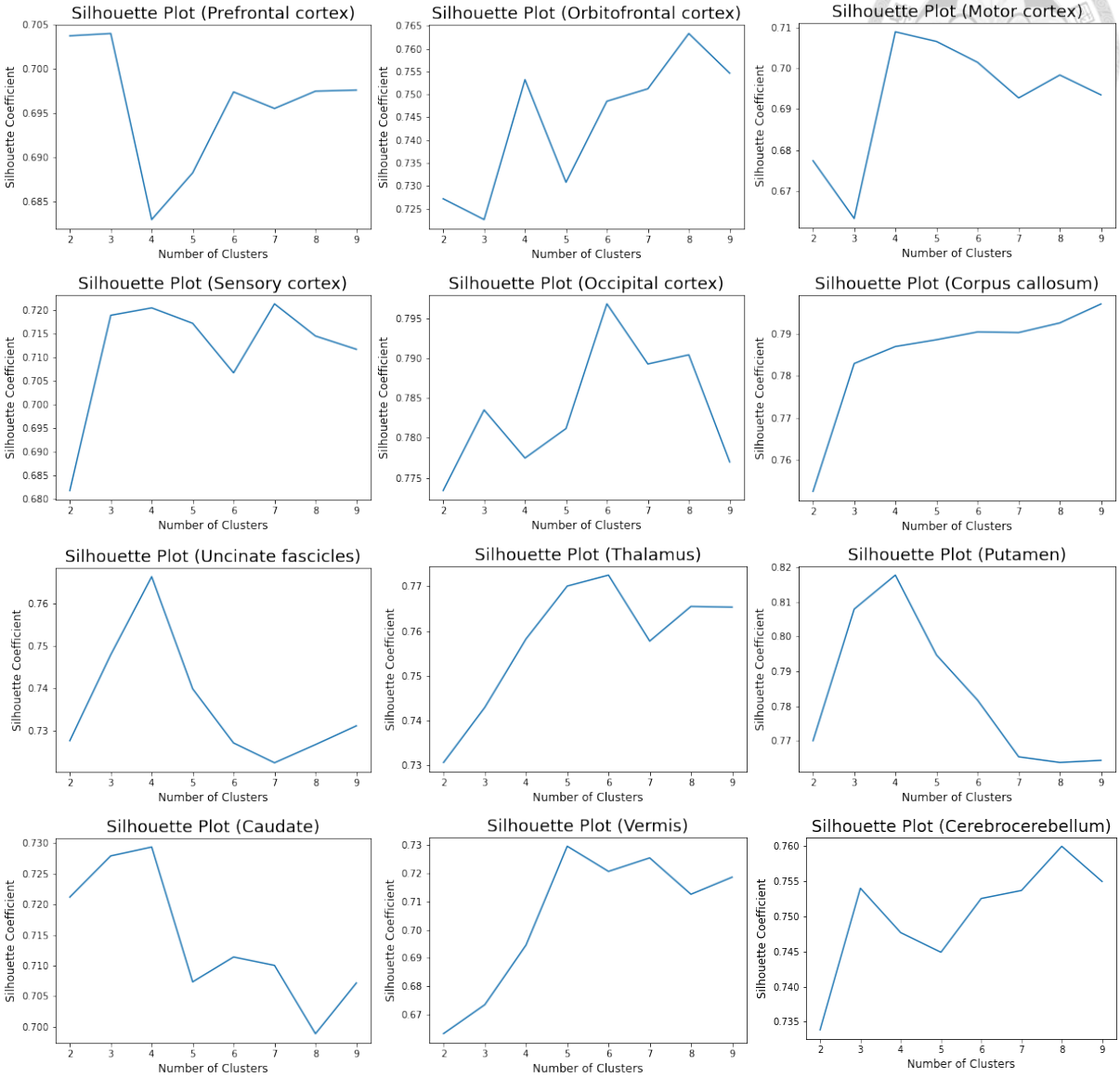

Figure 3.6 The silhouette plots for each brain region to determine the optimized number of clusters from 2 to 9 to avoid complexed clustering.

doi:10.6342/NTU202304442

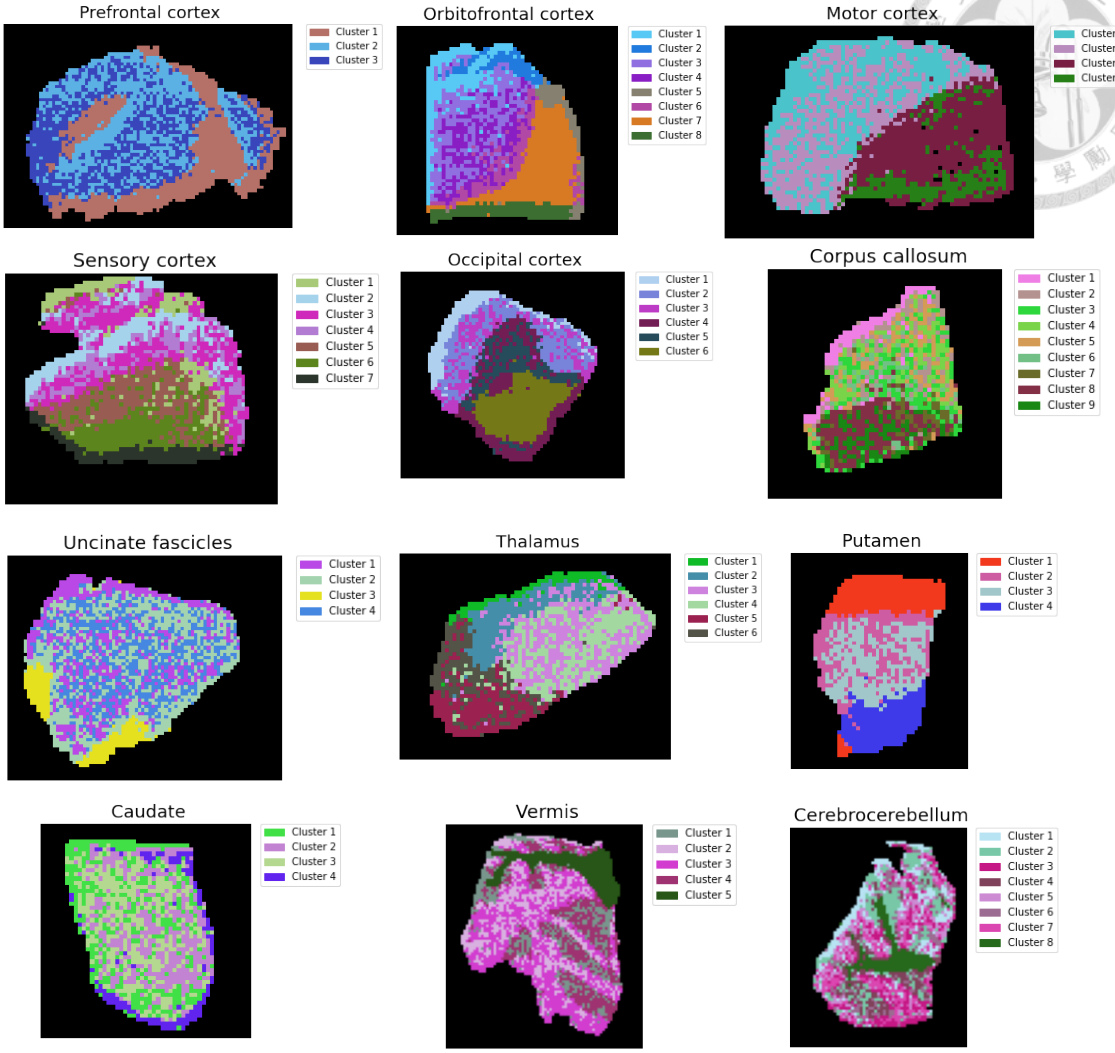

Figure 3.7 The clustering results of mass spectrometry images (left) after dimensionality reduction of the MSI data.

doi:10.6342/NTU202304442

3.3.2 The Distribution of α-Synuclein Accumulation across the 12 Brain Regions

We applied IHC staining to assess the severity of α-synuclein accumulation. After staining the tissues, we examined the level of α-synuclein aggregation particles in the 12 brain regions. Figure 3.8 shows the most intense visual field with the highest number of α-synuclein aggregation particles. As the density of aggregation particles cannot be directly visualized in the visual scale of the whole tissue, we applied a 500 μm*500 μm grid on the tissue and calculated the number of aggregation particles in each visual field to represent the level of α-synuclein accumulation. The severity of α-synuclein accumulation in the 12 brain regions is visualized in Figure 3.9. The two regions of the cerebellum and the two regions of the basal ganglia exhibited severe α-synuclein accumulation, followed by the motor cortex and thalamus. Other areas of the cerebral cortex only displayed a relatively slight accumulation of α-synuclein.

doi:10.6342/NTU202304442

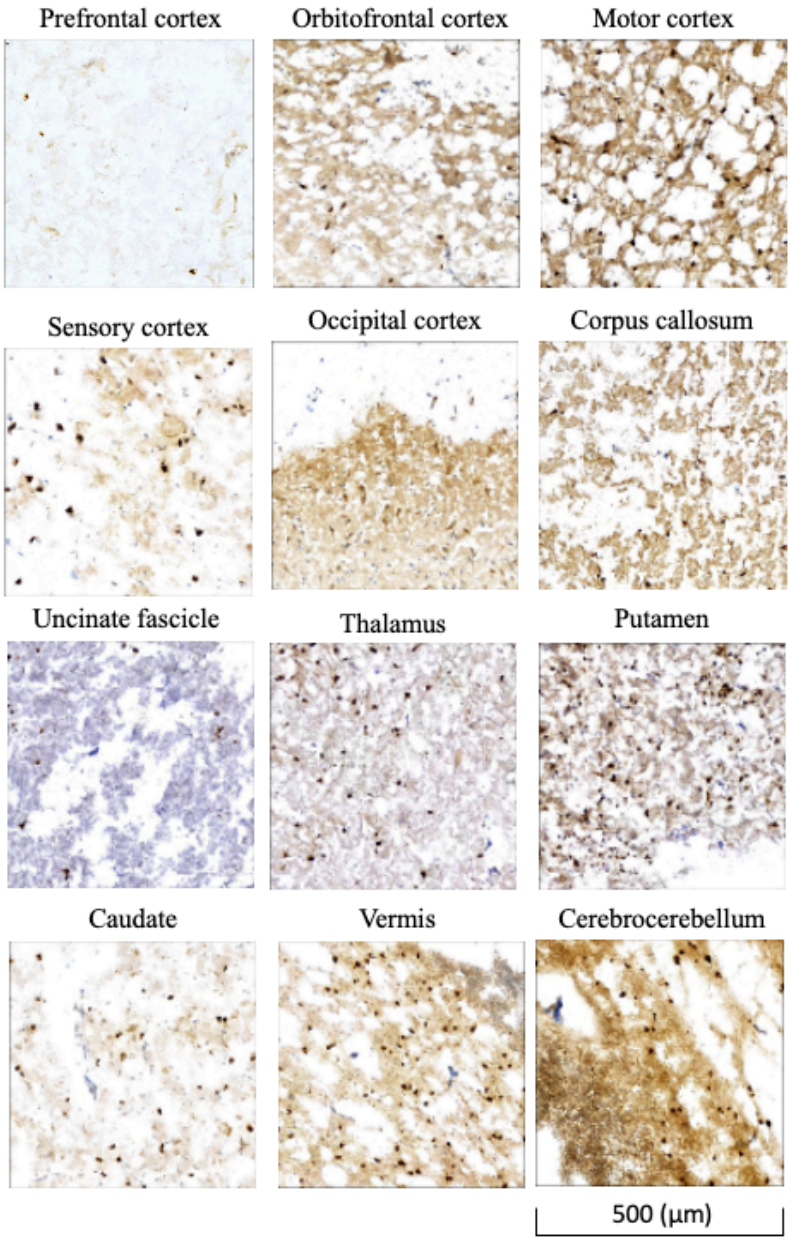

Figure 3.8 The most intensive visual field with the most aggregation particles of α-synuclein of the 12 brain regions in a 10x magnifying visual field.

doi:10.6342/NTU202304442

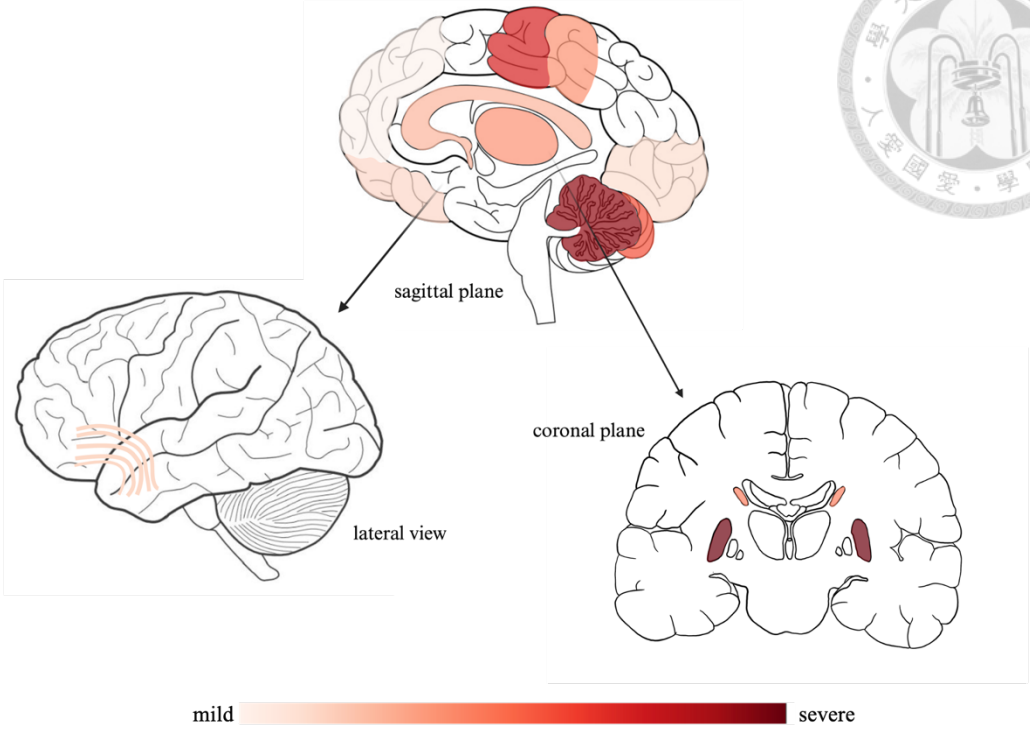

Figure 3.9 Summarizes the severity of α-synuclein accumulation in the 12 brain regions.

doi:10.6342/NTU202304442

3.3.3 The Spatial Correlation of α-Synuclein Accumulation and Lipid Distribution

In addition to the different levels of accumulation in different brain regions, there are also varying levels of α-synuclein accumulation in different areas of the tissue within one brain region. To visualize such differences, we calculated the amount of aggregation particles within each grid applied to the tissue and presented them in heatmap form. We found that the level of α-synuclein accumulation is consistent with the spectral pattern of mass spectrometry images of these MSA brain tissues, which indicated that the distribution of some metabolites was spatially correlated with the distribution of α-synuclein. Figure 3.10 shows the original staining results of the 11 MSA brain regions, the heatmaps of the amount of α-synuclein aggregation, the clustering results of mass spectrometry images, and the distribution of the lipids belonging to the cluster where the α-synuclein aggregations are more intensive. The results do not show the α-synuclein and lipid distribution in the prefrontal cortex, as there were few α-synuclein aggregation particles detected in the IHC staining of the prefrontal cortex. The distribution was not specific to a certain area of the tissue. In our findings, all the lipids that exhibited spatial correlation with α-synuclein accumulation belonged to ceramide, cerebroside, sulfatide, and phosphatidylserine species. On the other hand, no unsaturated fatty acids showed a spatial correlation with α-synuclein accumulation. Table 3.3 summarizes the lipids spatially correlated with α-synuclein accumulation in the 12 brain regions.

doi:10.6342/NTU202304442

(a) Orbitofrontal cortex

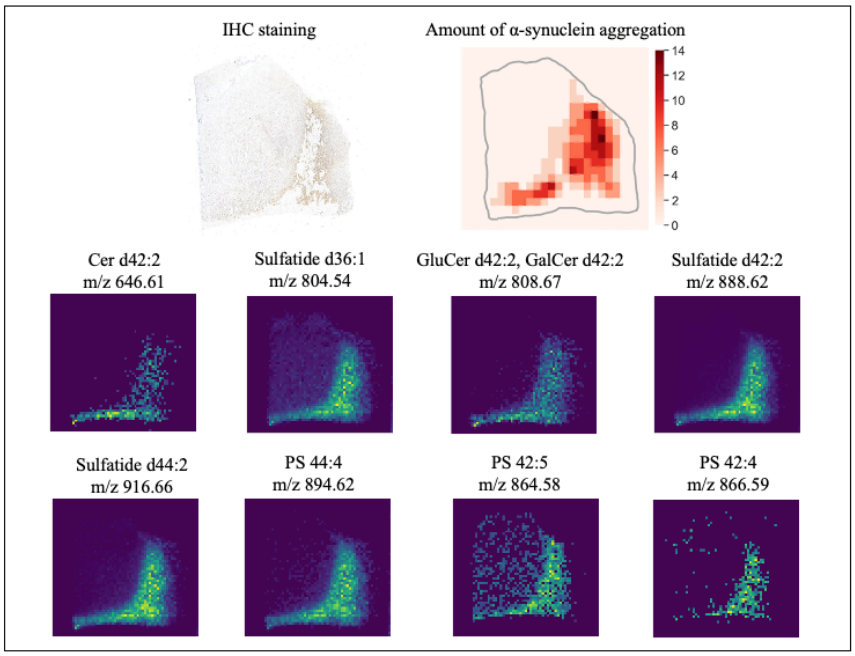

(b) Motor cortex

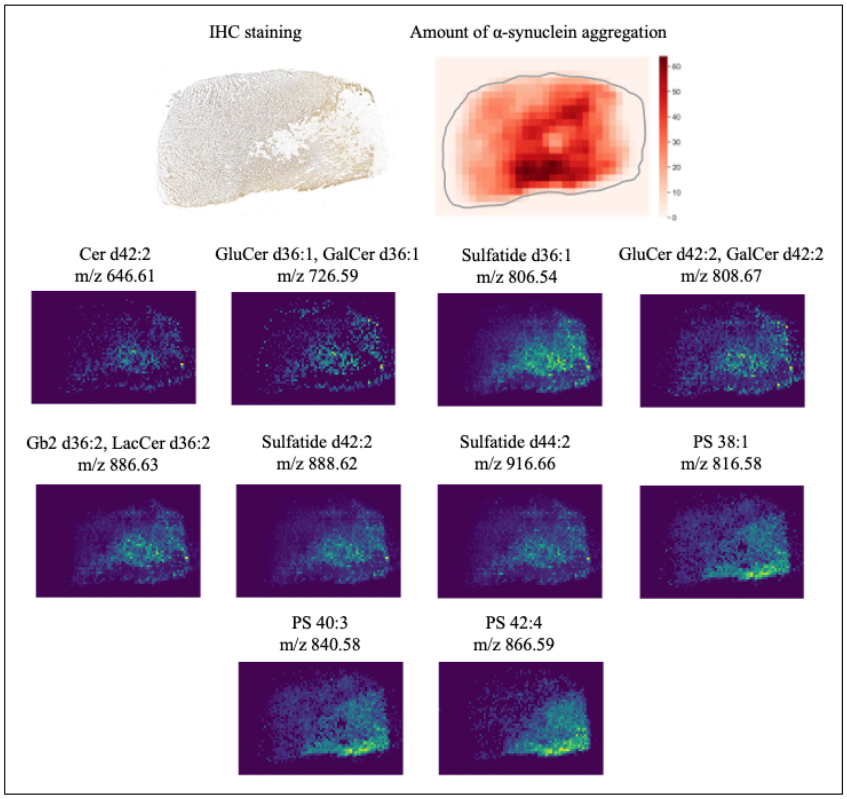

doi:10.6342/NTU202304442

(c) Sensory cortex

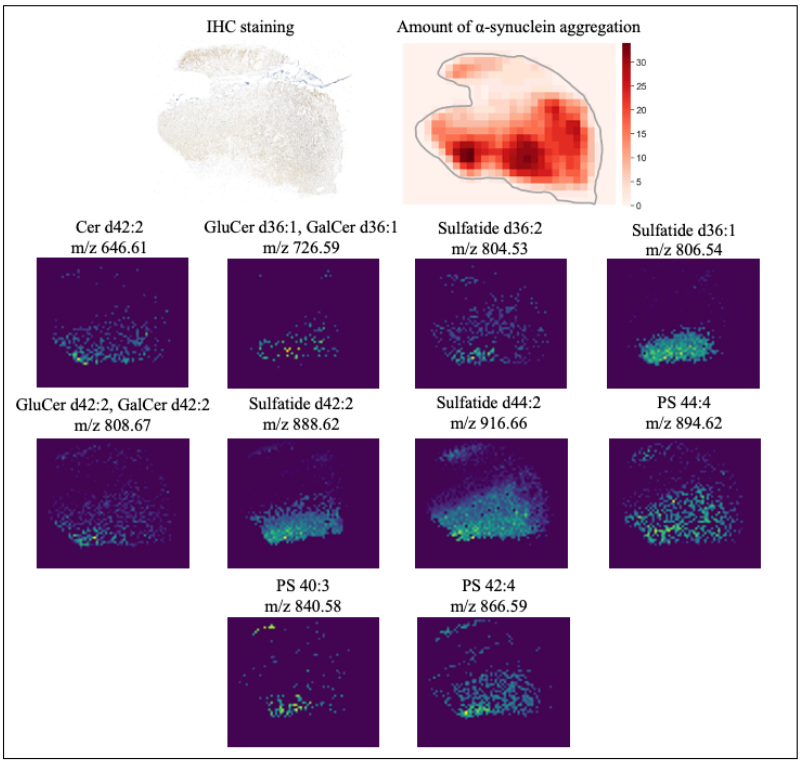

(d) Occipital cortex

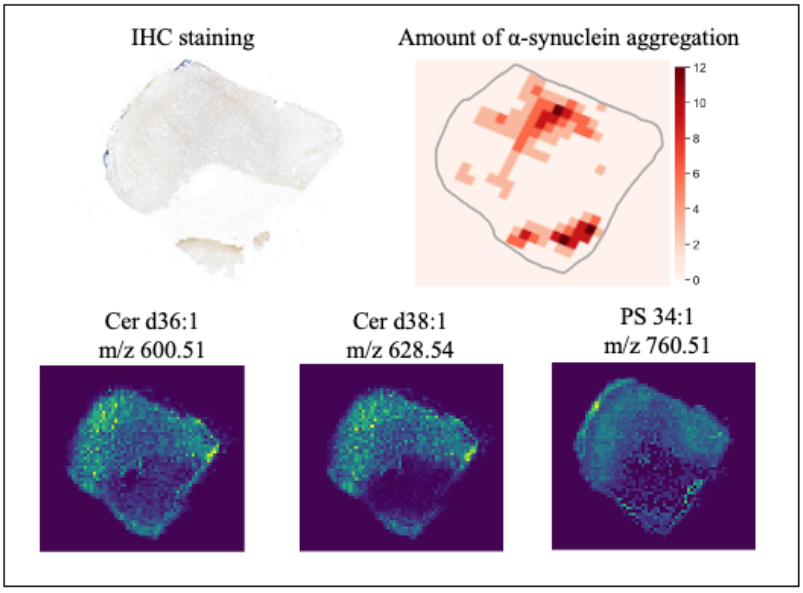

doi:10.6342/NTU202304442

(e) Corpus callosum

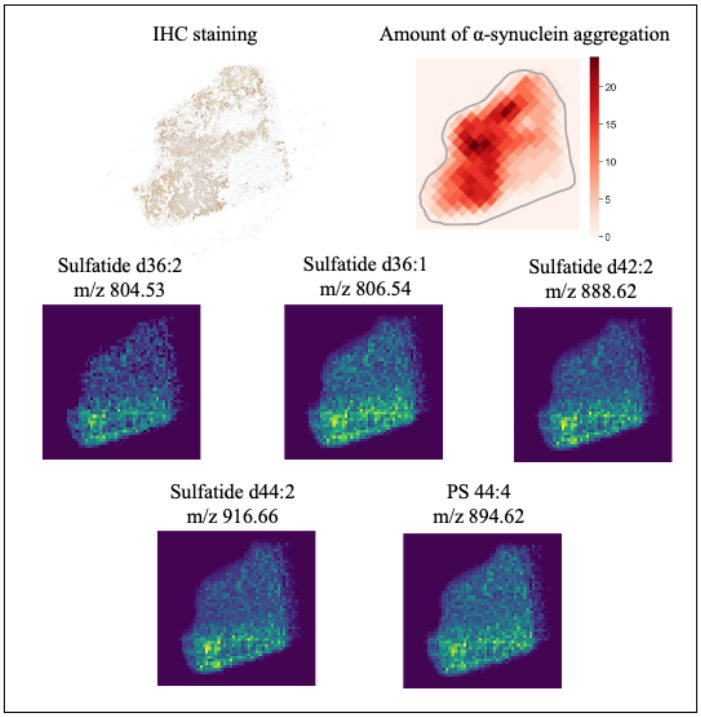

(f) Uncinate fascicle

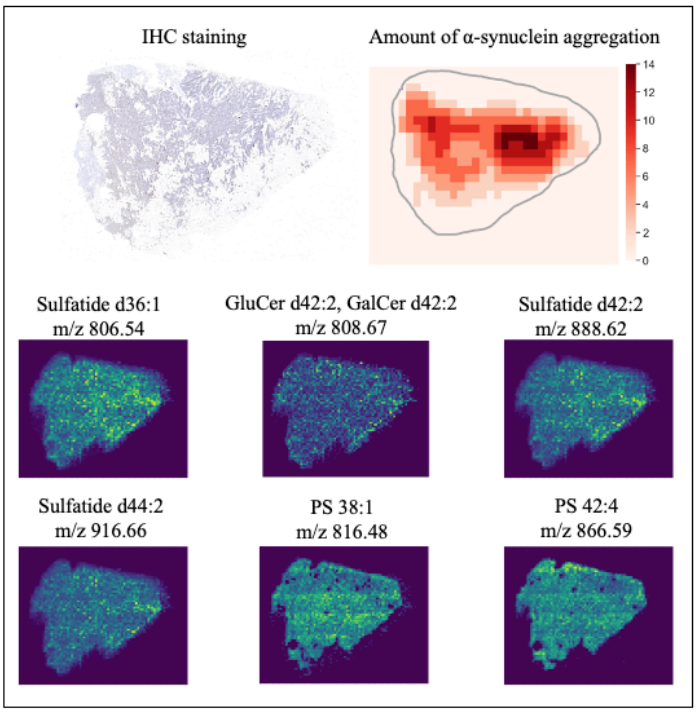

doi:10.6342/NTU202304442

(g) Thalamus

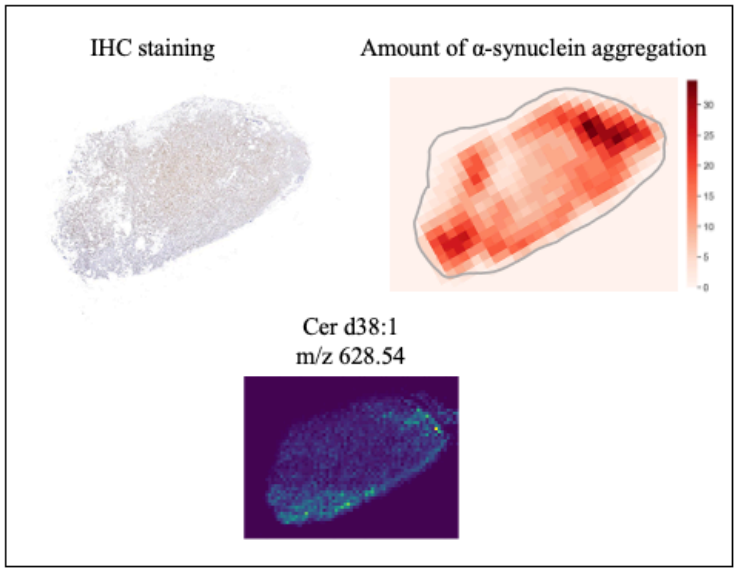

(h) Putamen

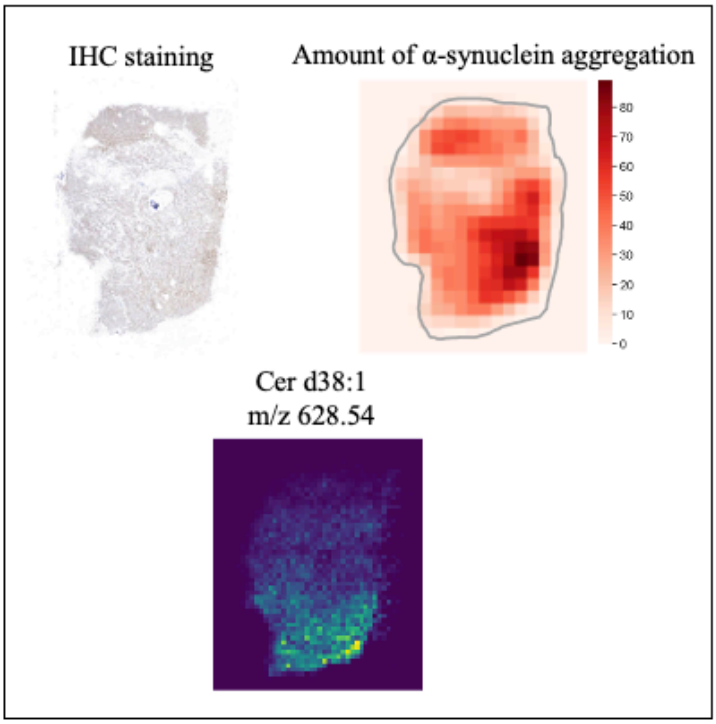

doi:10.6342/NTU202304442

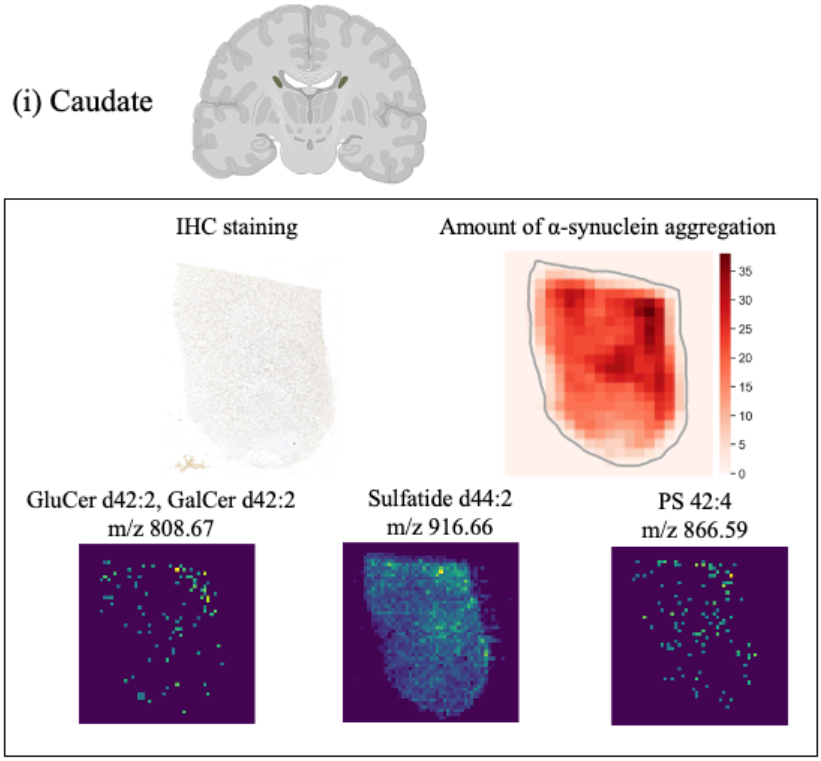

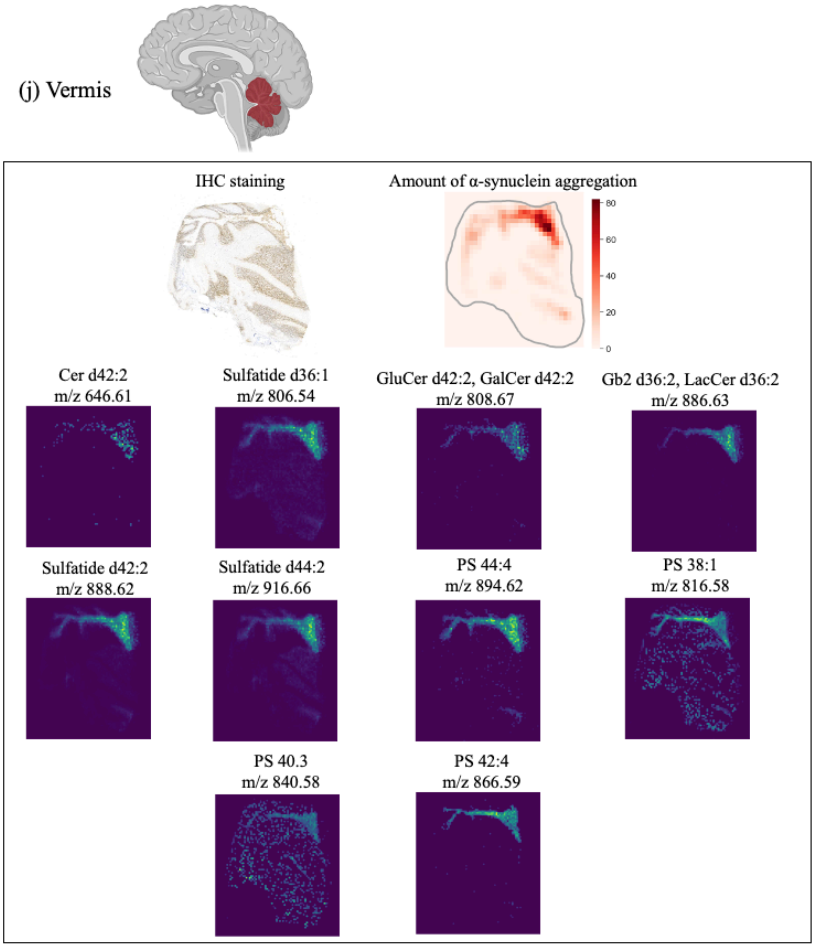

doi:10.6342/NTU202304442

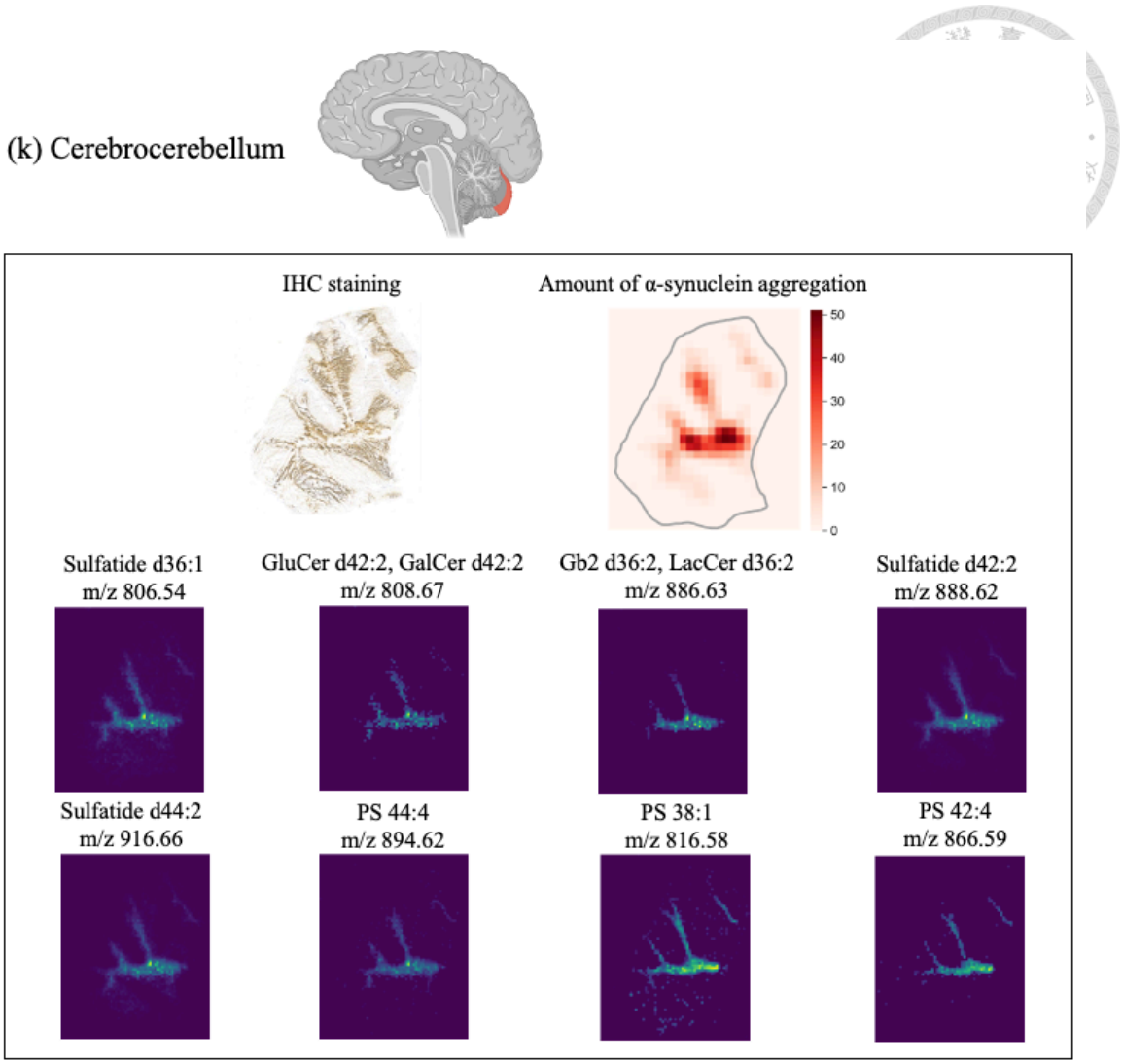

Figure 3.10 The original staining results of the 12 MSA brain regions, the heatmaps of the amount of α-synuclein aggregation, the clustering results of mass spectrometry images after dimensionality reduction, and the distribution of the spatially correlated lipids.

doi:10.6342/NTU202304442

Table 3.3 Summary of the lipids that showed spatial correlation with α-synuclein accumulation in the 12 brain regions in the MSA group.

	Ceramide	Cerebroside	Sulfatide	Phosphatidylserine
Prefrontal cortex	-	-	-	-
Orbitofrontal cortex	d42:2	GluCer d42:2, GalCer d42:2	d36:1, d42:2, d44:2	44:4, 42:4, 42:5
Motor cortex	d42:2	GluCer d36:1, GalCer d36:1 GluCer d42:2, GalCer d42:2, Gb2 d36:2, LacCer d36:2	d36:1, d42:2, d44:2	38:1, 40:3, 42:4
Sensory cortex	d42:2	GluCer d36:1, GalCer d36:1, GluCer d42:2, GalCer d42:2	d36:2, d36:1, d42:2, d44:2	40:3, 42:4, 44:4
Occipital cortex	d36:1, d38:1	-	-	34:1
Corpus callosum	-	-	d36:2, d36:1, d42:2, d44:2	44:4
Uncinate fascicle	-	GluCer d42:2, GalCer d42:2	d36:1, d42:2, d44:2	38:1, 42:4
Thalamus	d38:1	-	-	-
Putamen	d38:1	-	-	-
Caudate	-	GluCer d42:2, GalCer d42:2	d44:2	42:4
Vermis	d42:2	GluCer d42:2, GalCer d42:2, Gb2 d36:2, LacCer d36:2	d36:1, d42:2, d44:2	44:4, 38:1, 40:3, 42:4
Cerebrocerebellum	-	GluCer d42:2, GalCer d42:2, Gb2 d36:2, LacCer d36:2	d36:1, d42:2, d44:2	44:4, 38:1, 42:4

doi:10.6342/NTU202304442

We further observed the expression pattern of the lipids that spatially correlated with α-synuclein and compared the expression pattern between the control and MSA groups. We identified pattern changes in the orbitofrontal cortex, motor cortex, thalamus, caudate, vermis, and cerebrocerebellum, as shown in Figure 3.11. The changes are not necessarily correlated with the severity of α-synuclein accumulation. The putamen, for example, underwent severe accumulation of α-synuclein, but the expression pattern of these lipids did not change between the two groups. However, the brain regions with clear pattern changes are all well-known as the most affected brain regions in the MSA disease progression. In the orbitofrontal cortex, motor cortex, and thalamus, ceramide d36:1 was the dominant lipid in the control group. At the same time, sulfatide d42:2 was dominant lipid in the MSA group, indicating that ceramide d36:1 is relatively less abundant and sulfatide d42:2 is relatively more abundant in the three brain regions. In contrast, the caudate, vermis, and cerebrocerebellum showed the opposite lipid expression patterns.

doi:10.6342/NTU202304442

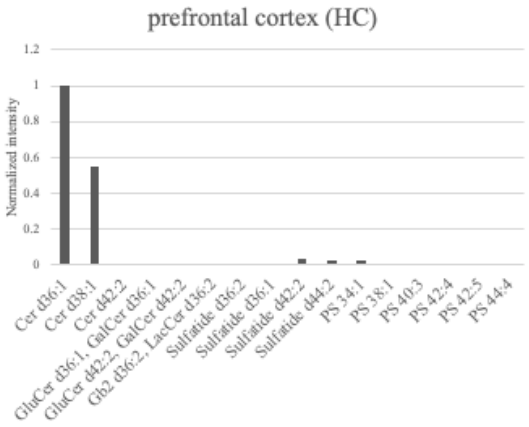

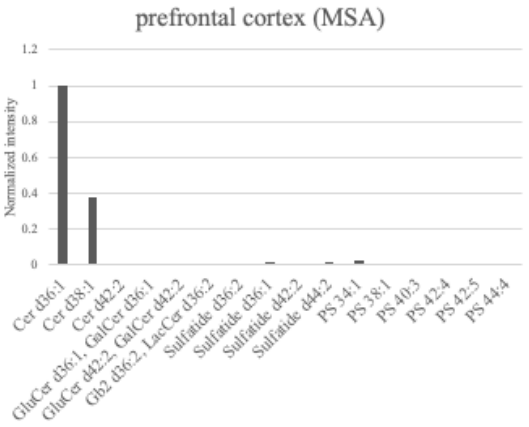

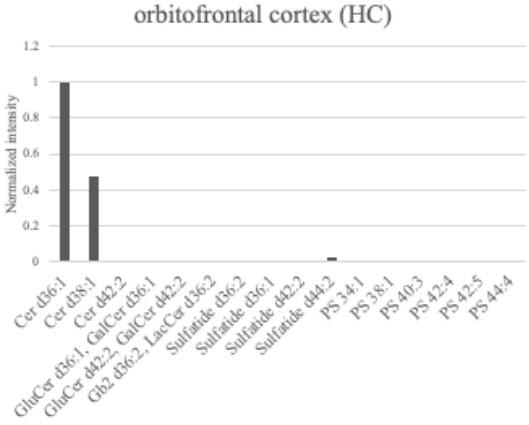

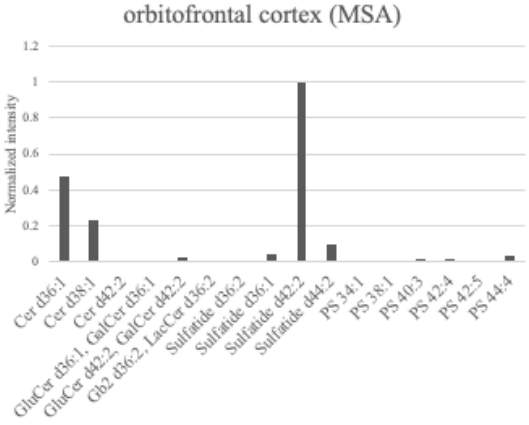

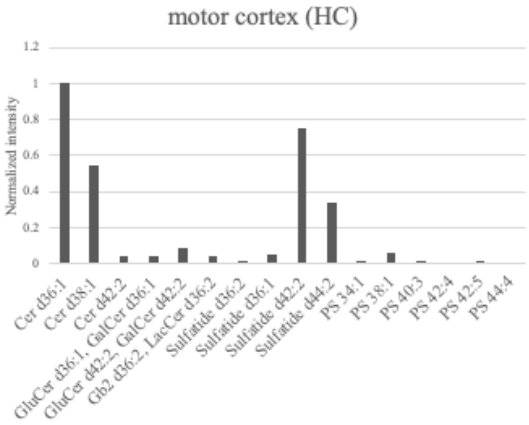

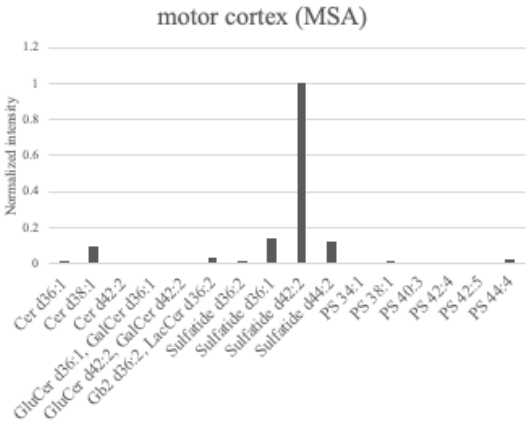

doi:10.6342/NTU202304442

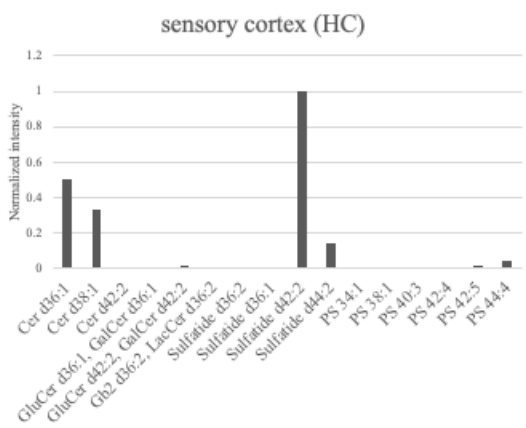

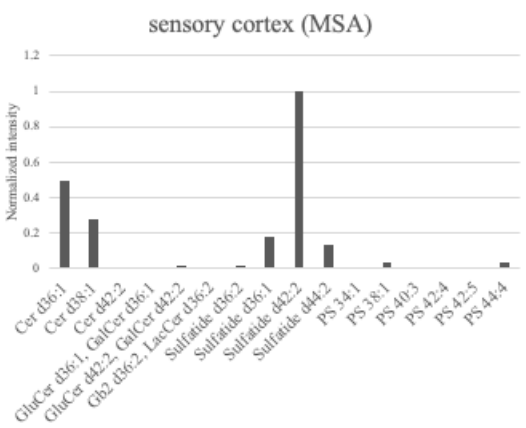

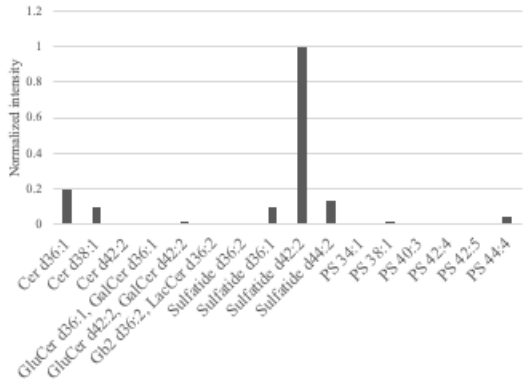

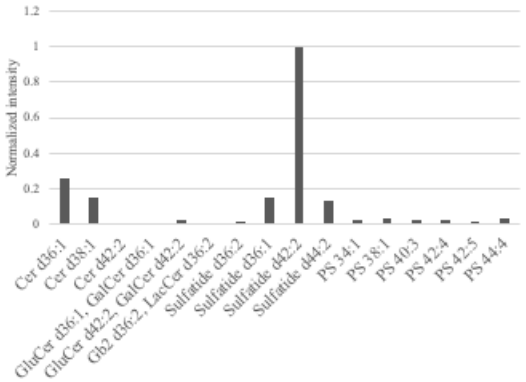

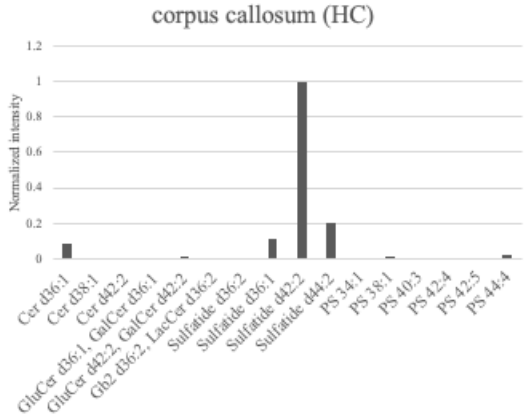

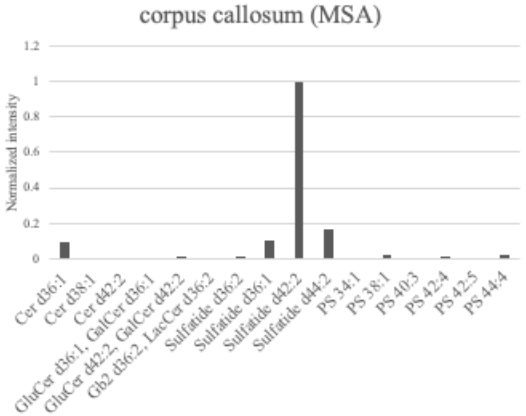

doi:10.6342/NTU202304442

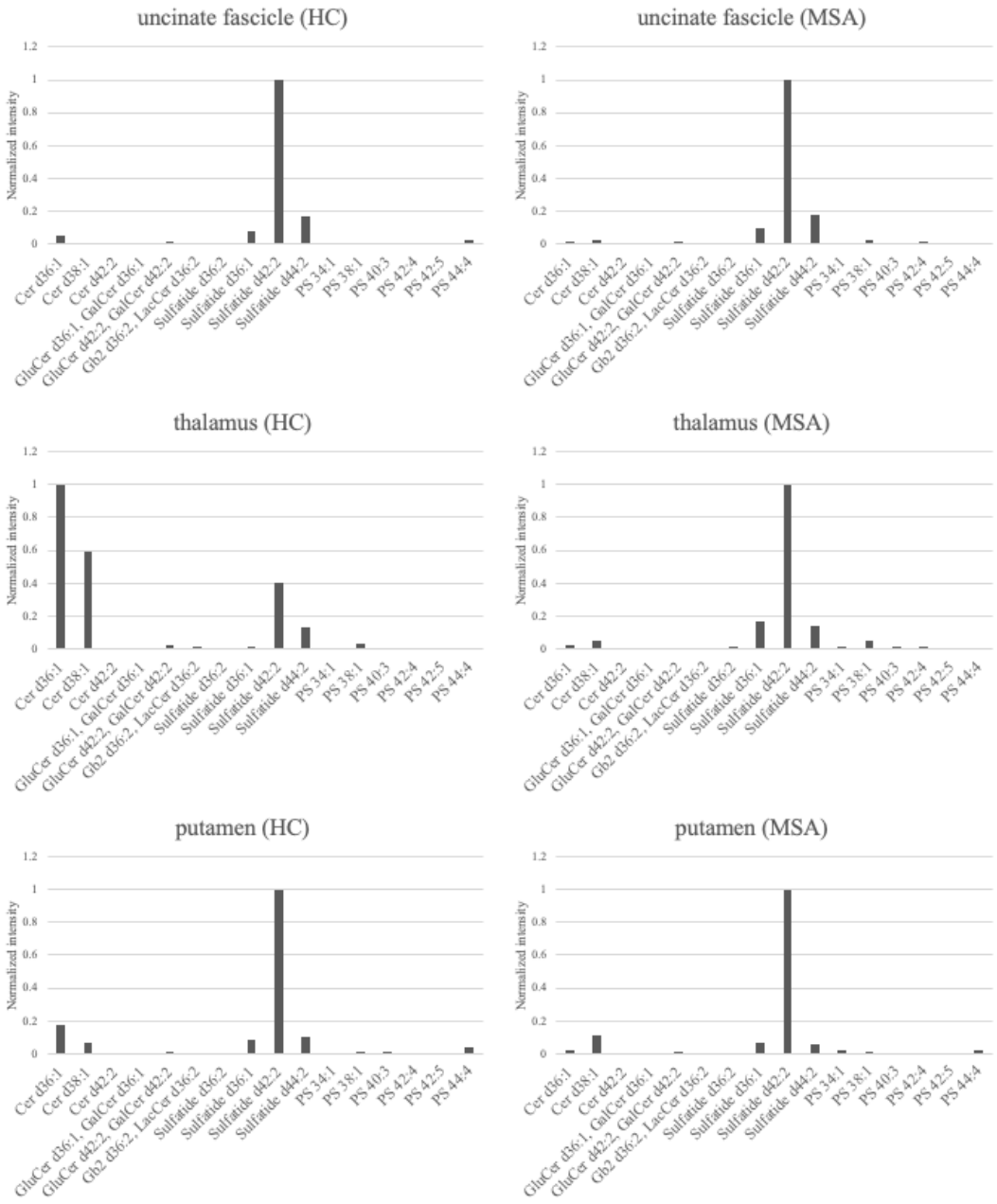

doi:10.6342/NTU202304442

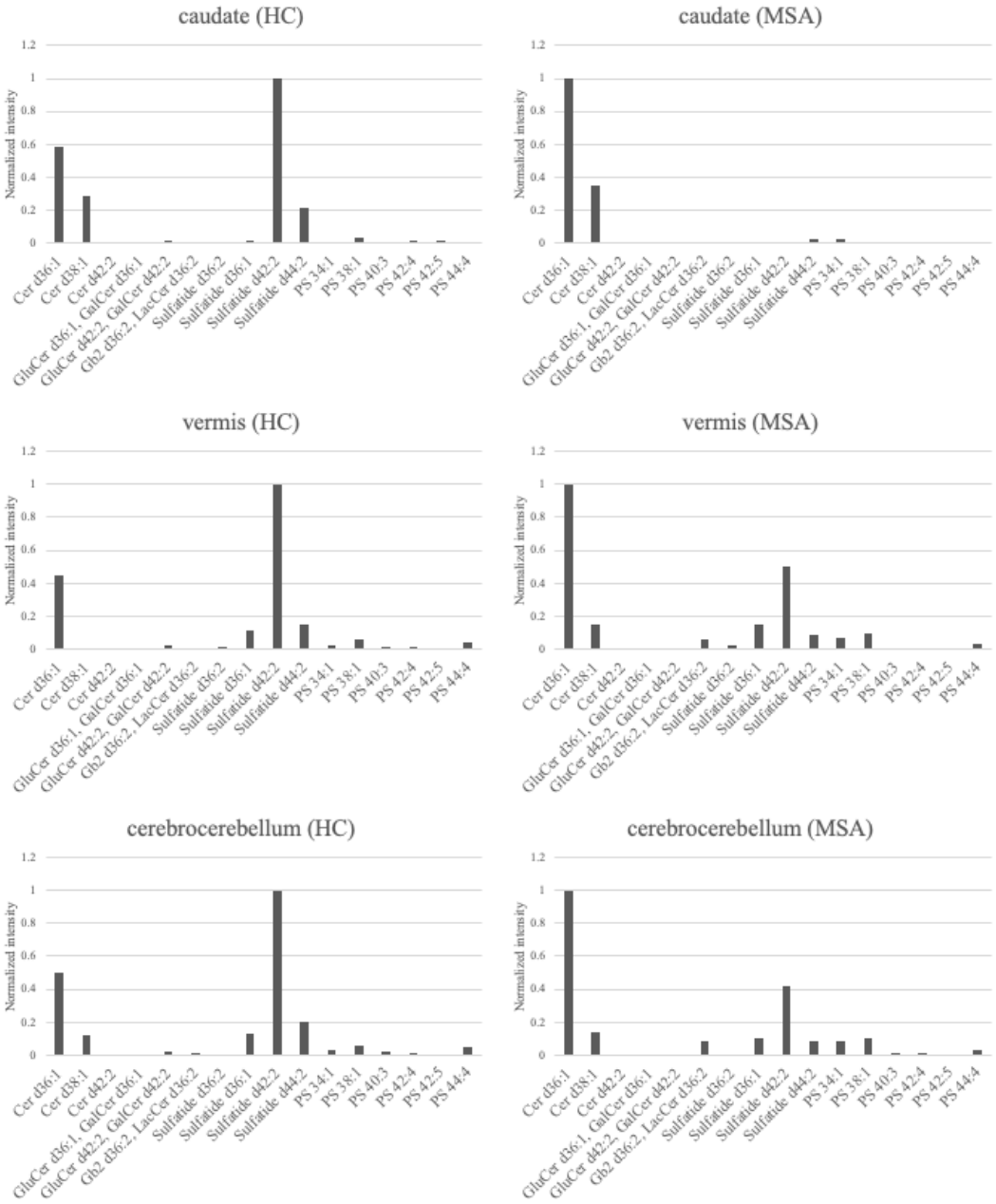

Figure 3.11 The normalized intensity of the lipids that spatially correlated with α-synuclein in the control (left) and MSA groups (right).

doi:10.6342/NTU202304442

Chapter 4 Discussion

4.1 Major Observations

4.1.1 DESI-MSI can be used to quickly construct and assess spatial molecular changes in tissue

The utility of DESI-MSI for detecting MSA-related metabolites was the main goal, as the instrument's resolution is limited compared to traditional mass spectrometry. First, we performed metabolite annotation and preliminary statistical analysis. As shown in Table 3.1, we found differential expression of lipids that were previously investigated, such as eicosapentaenoic acid in CSF[21], phospholipids[22][26], sphingomyelin, ceramide, and sulfatide species in plasma, lipid extract of the motor cortex and amygdala[23][25]. It is reasonable that the alteration of these lipids varied among different types of specimens; therefore, as long as we can detect the significantly expressed lipids found by more accurate methodologies, such as LC/MS-MS, the utility of DESI-MSI for lipidomic analysis can be confirmed. By referencing the literature, we demonstrated the effectiveness of DESI-MSI in analyzing changes in MSA-related lipids in brain tissues with a simple sample preparation process and minimal tissue damage.

Although studies have shown that most human brain regions share a common feature of lipid composition, there are still minor differences among brain regions.[58] Additionally, MSA can have varying degrees of influence on structural atrophy and lipid expression in different brain regions.[25] In this study, we used 12 brain regions as 12 samples in both the MSA and the control groups, so some of the minor changes across these brain regions may need to be addressed within the scope of differential testing. This discrepancy needs to be further clarified.

doi:10.6342/NTU202304442

4.1.2 Pathway Analysis Revealed Different Patterns of Lipid Changes among Brain Regions

To investigate the actual biological functions that were affected by MSA, the pathway analysis against the KEGG pathway and PubChem pathway databases was performed with the input lists containing the differentially expressed lipids. The results revealed the three most affected lipid metabolic pathways: sphingolipid metabolism, glycerophospholipid metabolism, and unsaturated fatty acid biosynthesis, as shown in Table 3.2. Then, we looked closer at the expression of all lipids involved in the three pathways we detected. (Figure 3.3~Figure 3.5)

Sphingolipids are a group of lipid classes that contain a sphingoid base backbone in their chemical structure. Ceramide is a relatively simple-structured class of sphingolipid. Several chemical modifications to ceramide can form other complex sphingolipids. For example, a ceramide with a phosphocholine or phosphoethanolamine structure forms a sphingomyelin. Glycosylated ceramides are referred to as cerebrosides, including glucosylceramide, galactosylceramide, and others; a sulfated cerebroside becomes a sulfatide, also known as 3-O-sulfogalactosylceramide. Functionally, sphingolipids, such as sphingomyelin, ceramides, and cerebrosides, regulate neuronal cell growth, programmed death, and neuroinflammation.[59][60][61] Sulfatide is essential for myelin maintenance[62]. In the work of Don *et al.*, the level of sulfatide was 4-fold higher in white matter under the motor cortex than in the visual cortex. In contrast, in the MSA group, whose motor cortex is affected by MSA, the level of sulfatide is only 2.7-fold higher. The MSA group also showed an overall decrease in sulfatide levels compared with the control group. They assumed that lipid changes cause myelin instability and degeneration.[25] However, the expression of sphingolipids is finely regulated in the

doi:10.6342/NTU202304442

healthy human brain. While decreased expression of ceramides may hinder the early growth of neuronal cells, overexpression can also lead to neuroinflammation, neuronal death, and abnormal myelination.[63] Additionally, other studies have indicated that overexpression of sulfatide species may lead to an inhibition of oligodendrocyte differentiation and axon growth despite the myelin-maintaining function of sulfatide in the healthy human brain.[64] As shown in Figure 4.1, in our study, there were significant increases in sulfatide species expression in the cerebral cortex, such as in the orbitofrontal cortex, motor cortex, and sensory cortex, as well as in the thalamus, where the neural fibers project out to connect to the cerebral cortex. This suggested a possible loss of motor function due to oligodendrocyte differentiation inhibition caused by MSA. Our results showed an opposite trend compared to that demonstrated in Don's work, mainly due to the specimen type, which was the white matter in Don's work and the cerebral cortex in our study. Therefore, the conflicting trends may be due to the rearrangement of lipid distribution in neural cells, which needs to be further clarified.

doi:10.6342/NTU202304442

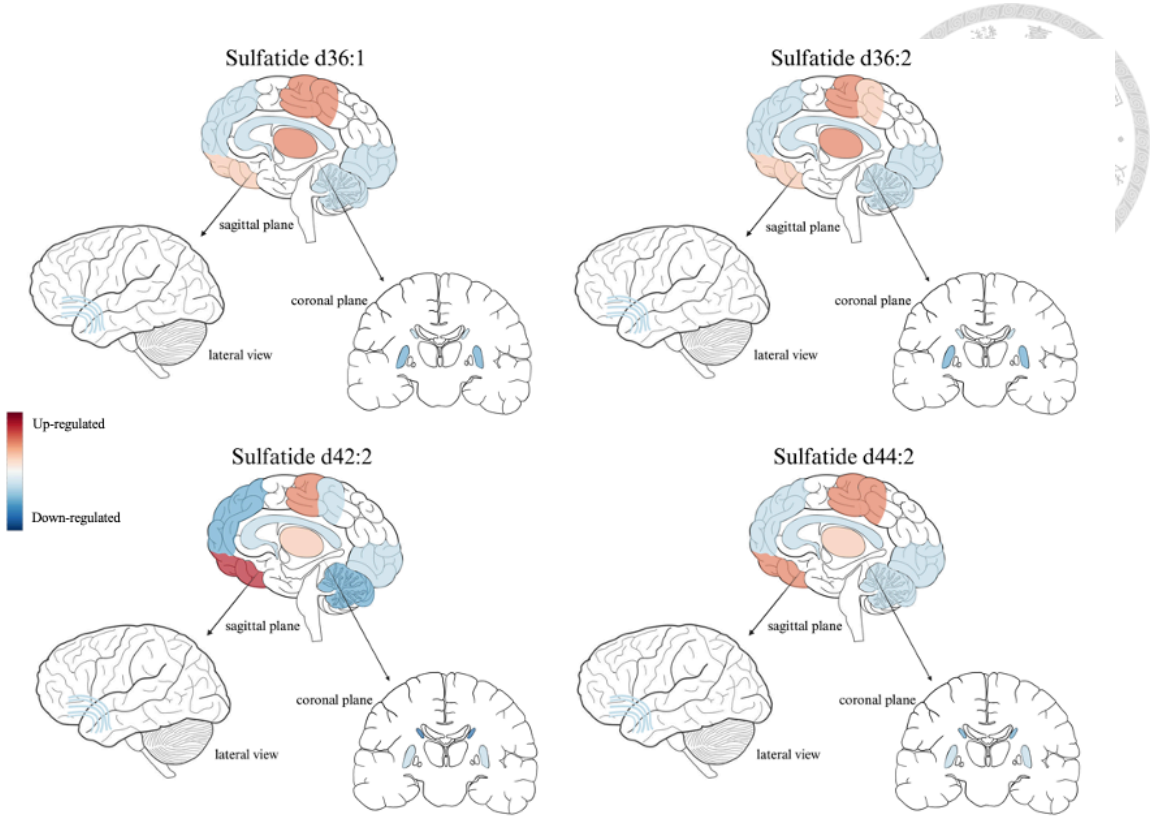

Figure 4.1 The expression trends of sulfatide species in the 12 brain regions from the MSA group compared to the healthy control group.

Glycerophospholipids, including phosphatidic acid, phosphatidylcholine, phosphatidylserine, and phosphatidylethanolamine, are essential components of biological membranes, and they maintain the stability and fluidity of the membrane. They also signal apoptosis and phagocytosis by translocating between inner and outer cell membranes. Most glycerophospholipid species can bind with α-synuclein[16] and cause subsequent aggregation on the lipid bilayer of the neural cell membrane, which may contribute to neural death due to abnormal membrane permeability. In the work of Fu *et al*., the authors found the overall elevation of several unsaturated glycerophospholipids, such as PC, PE, and PC, regardless of the length of the acyl chain and the number of double bonds, in the amygdala where abnormal α-synuclein accumulation was identified.[26] In our findings, the alteration of different species with varying lengths of

doi:10.6342/NTU202304442

acyl chains within the lipid classes of phosphatidic acid, phosphatidylethanolamine, and phosphatidylcholine were inconsistent. However, some phosphatidylserine species still showed a specific alteration pattern across brain regions. In Figure 4.2, we found significant elevation of PS 38:1, PS 40:3, PS 42:4, and PS 42:5 in the orbitofrontal cortex, motor cortex, sensory cortex, and thalamus and minor elevation in the prefrontal cortex, occipital cortex, corpus callosum, uncinate fascicles, and cerebellum. Typically, PS species are more abundant in the inner layer of the cell membrane; the flipping of PS species from the inner membrane to the outer membrane can trigger the initiation of the apoptosis mechanism. As a result, the overexposure of PS species in the outer membrane is considered an 'eat-me' signal that leads to downstream phagocytosis. Programmed death has been implicated in the progressive loss of neurons and the pathogenesis of neurodegenerative diseases.[65] Additionally, increased phosphatidylserine and α-synuclein binding can impair cell membrane permeability. Our results showed the same trends of alteration of PS species as in the work of Fu *et al.* Although we did not include the amygdala in any of the target brain regions in our study, some brain regions that interact strongly with the amygdala, such as the corpus callosum and thalamus, still showed consistent alteration of PS species with that exhibited by the amygdala in the study by Fu *et al*. The putamen and caudate are also structurally and functionally connected to the amygdala; however, our studies demonstrated that the alteration of PS in these two regions changed in different species with varying acyl chain lengths and numbers of double bonds.

doi:10.6342/NTU202304442

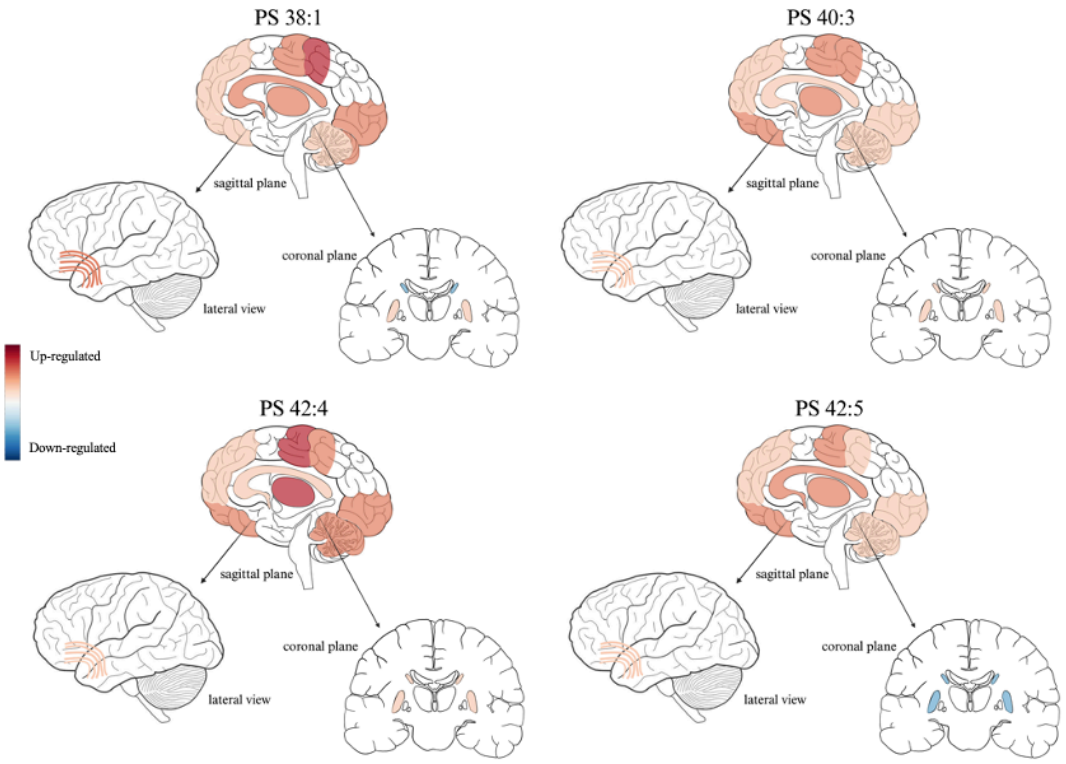

Figure 4.2 Phosphatidylserine species' expression trends in the 12 brain regions from the MSA group compared to those of the healthy control.

Fatty acids are an essential lipid class found in the human brain, and many of them are essential fatty acids, meaning that we require exogenous ingestion to keep the body functioning normally. Most of these essential fatty acids are polyunsaturated fatty acids (PUFAs), including ω−3 and ω−6 fatty acids. These two types of fatty acids serve as inflammatory mediators. Typically, ω−3 and ω−6 fatty acids share several fatty acyl-CoAs as common upstream chemical materials. Hence, the expression of these two types of fatty acids is in balance, and this relationship also reflects their roles in regulating inflammation. ω−3 fatty acids, such as eicosapentaenoic acid (EPA), docosapentaenoic acid 22n-3 (DPA 22n-3), docosahexaenoic acid (DHA), are known to have anti-inflammation activity.[68] Some ω−6 fatty acids, on the other hand, can promote inflammation, as they act as the precursors to proinflammatory mediators, such as linoleic

doi:10.6342/NTU202304442

acid (LA), arachidonic acid (ARA), adrenic acid (AdA), docosapentaenoic acid 22n-6 (DPA 22n-6), tetracosatetraenoic acid (TTA), and tetracosapentaenoic acid (TPA).[69] Lee *et al*. identified EPA as a marker that elevated CSF in MSA patients. In contrast, our findings demonstrated an overall elevation of EPA among most brain regions. At the same time, some other detected ω−6 fatty acids, such as docosapentaenoic acid 22n-6, tetracosapentaenoic acid 24:5n-6, and tetracosatetraenoic acid 24:4n-6, presented the opposite trends. These results were consistent with the previous findings that the patients with MSA might have a compensatory response to neuroinflammation, which caused the elevated levels of ω−3 fatty acids and decreased levels of ω−6 fatty acids. For EPA, there were varying degrees of the alteration, with the elevation being two to threefold in the natural logarithm scale compared to the control level in the basal ganglia and cerebellum, as shown in Figure 4.3; thus, among all MSA-affected brain regions, those in the basal ganglia and cerebellum may suffer more severe neuroinflammation. The alterations in these ω−3 and ω−6 fatty acids were different in the corpus callosum and thalamus. In the corpus callosum, TPA was elevated, while there were significant decreases in the levels of EPA, DPA, and TTA. In the thalamus, EPA and TTA were elevated, while DPA and TPA were decreased.

doi:10.6342/NTU202304442

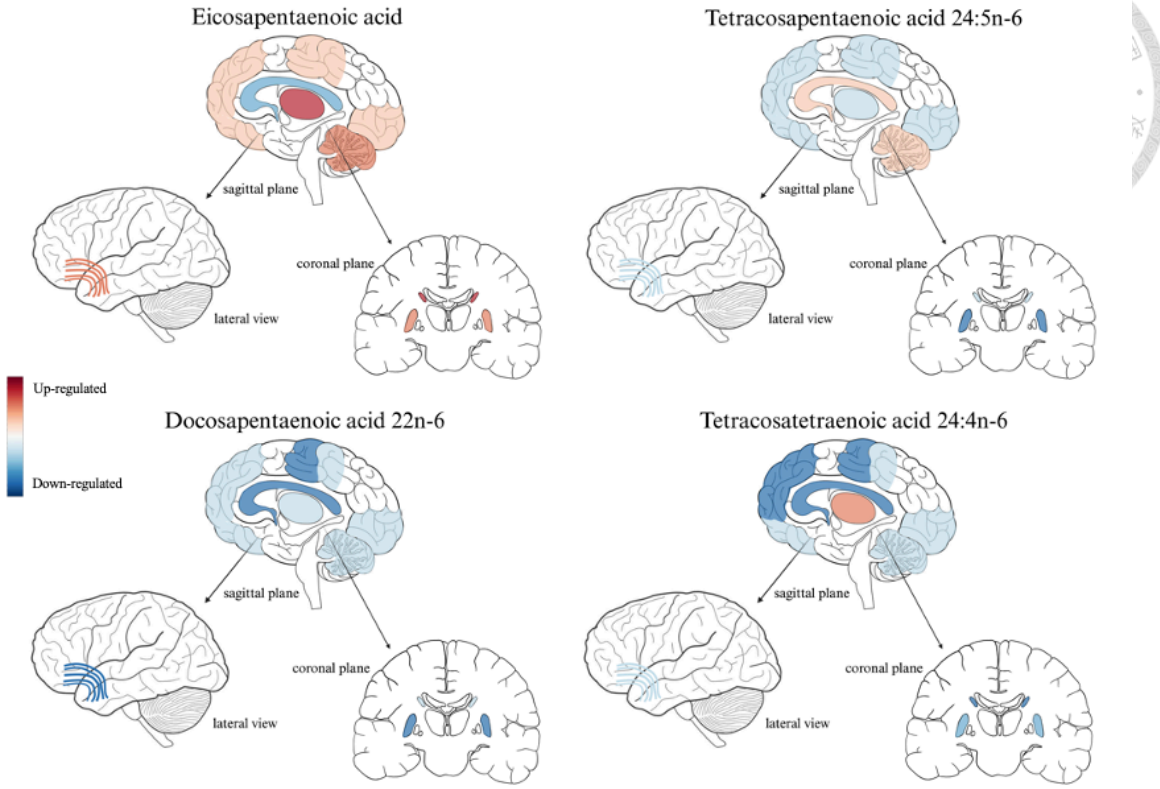

Figure 4.3 The trends of expression of unsaturated fatty acids in the 12 brain regions in the MSA group compared to those in the healthy control group.

4.1.3 The IHC staining Confirmed the Presence of α-Synuclein Accumulation in Different Brain Regions

In general, MSA can affect multiple brain regions such as the motor cortex, midbrain, basal ganglia, and cerebellum; moreover, the severity of neuronal loss typically follows the pathological hallmark of the aggregation of α-synuclein-positive GCIs in neural cells and fibers.[70] The neuronal loss caused by MSA-C starts in the midbrain and cerebellum, and then progresses to the basal ganglia, followed by the motor cortex over time. Disease severity is related to the progression of neuronal loss. Most MSA-C patients may experience mild motor cortex degeneration, moderate basal ganglia degeneration, and more severe deterioration of the cerebellum. In this study, the vermis of the cerebellum, the putamen, and the motor cortex demonstrated the most severe accumulation of α-

doi:10.6342/NTU202304442

synuclein (Figure 3.8 and Figure 3.9), which is consistent with the current understanding of the brain regions most affected by α-synuclein accumulation and may induce the main symptoms, such as unsteady gait, cognitive failure, and motor dysfunction. As the atrophy of these brain regions presents a more intensive accumulation of α-synuclein, while some of the neural-maintaining lipids, such as sphingolipid and glycerophospholipid, are significantly altered in these brain regions, it is important to clarify the lipid disturbances in these three brain regions, including the vermis of the cerebellum, putamen, and motor cortex.

4.1.4 Lipid Alterations Are Hypothesized to Be Related to General Clinical Presentations of MSA in Some Brain Regions

Our study included these most affected brain regions, and the results indicated different patterns of lipid alteration across brain regions. Some lipid alterations in MSA patients have been found to have relation with some general biochemical presentations of MSA in different brain regions. Here we discussed these lipid alterations in three different brain regions representing the brain regions in the cerebellum, basal ganglia, and cerebral cortex, and generated hypothesis of the changes of the biochemical functions inducing by the lipid alterations that we have detected in our study.

The cerebellum, which plays a vital role in motor control and coordination, is usually the first region where neuronal loss is initiated in the brain in a patient with MSA. The symptoms of cerebellar degeneration, such as unsteady gait and loss of balance, are the most distinct features found in patients with MSA.[15] Figure 4.4 summarizes the lipid alterations in the vermis of the cerebellum regarding the three lipid metabolic pathways: sphingolipid metabolism and biosynthesis of unsaturated fatty acids, based on an absolute

doi:10.6342/NTU202304442

ln-fold change > 1.5, which were considered differentially expressed between the two groups. The results showed that in the cerebellar vermis, where the neuronal loss is supposed to be the most severe, the EPA, ceramide, and cerebroside species are significantly elevated in patients with MSA. At the same time, there is little difference in the level of sulfatide species. As described in section 4.1.2, EPA regulates neuroinflammation as compensation for the affected neural cells. At the same time, elevation of ceramide species can induce neuroinflammation by excessively inhibiting the Akt/mTOR pathway.[71] We hypothesize that the late stage of MSA progression has causes severe neuroinflammation in the cerebellum.

Following the cerebellum, the basal ganglia, including the putamen, caudate, and others, are usually the next group of brain regions affected by MSA progression. The basal ganglia are located at the top of the midbrain and are structurally and functionally interconnected with the cerebral cortex, thalamus, and brainstem. They control the autonomic motor function and some advanced integrated consciousness, such as conditional learning, cognition, and memory.[72] Figure 4.5 shows the lipid alterations in the putamen, which is representative of the basal ganglia in this study, regarding the three lipid metabolic pathways. In the putamen, there are significant elevations in EPA, meaning that neuroinflammation has occurred in these two regions. Moreover, decreases in the levels of cerebroside and sulfatide species can hinder neural growth.[59] The late stage of MSA progression has induces neuroinflammation, and the inhibition of neural growth still occurs in the caudate.

The motor cortex is the latest brain region most recently affected by MSA. Usually, the motor cortex serves as the primary motor unit to generate the movement signal to the body. In Figure 4.6, our results showed no significant difference in the level of EPA between the two groups, suggesting a lower tendency of neuroinflammation happening

doi:10.6342/NTU202304442

in the motor cortex. Nevertheless, the levels of ceramide species are significantly decreased, resulting in insufficient regulation of the Akt/mTOR pathway which can induce the activation of some programmed cell death procedures such as apoptosis and autophagy. The sulfatide species is elevated considerably in the MSA group, indicating the inhibition of neural outgrowth in the motor cortex.

On the other hand, the alteration of glycerophospholipid, such as PA, PC, and PE species, showed little consistency among different species within a lipid class. According to Fu's work[26], total PC, PE, and PS classed demonstrated elevated values, while the alteration of each species was left uncleared; thus, comparing our results to those of their study was difficult. Therefore, the alteration of different PA, PC, and PE species in other brain regions may need thorough investigation to be further clarified. However, our results (Figure 3.4b) showed that the PS class level is elevated in the motor cortex which can also promote the phagocytosis events in the programmed cell death procedure. Additionally, the elevation of PS species can enhance the abnormal accumulation of α-synuclein. Compared to that in the control group, there was little difference in PS expression in the cerebellum in the MSA group.

doi:10.6342/NTU202304442

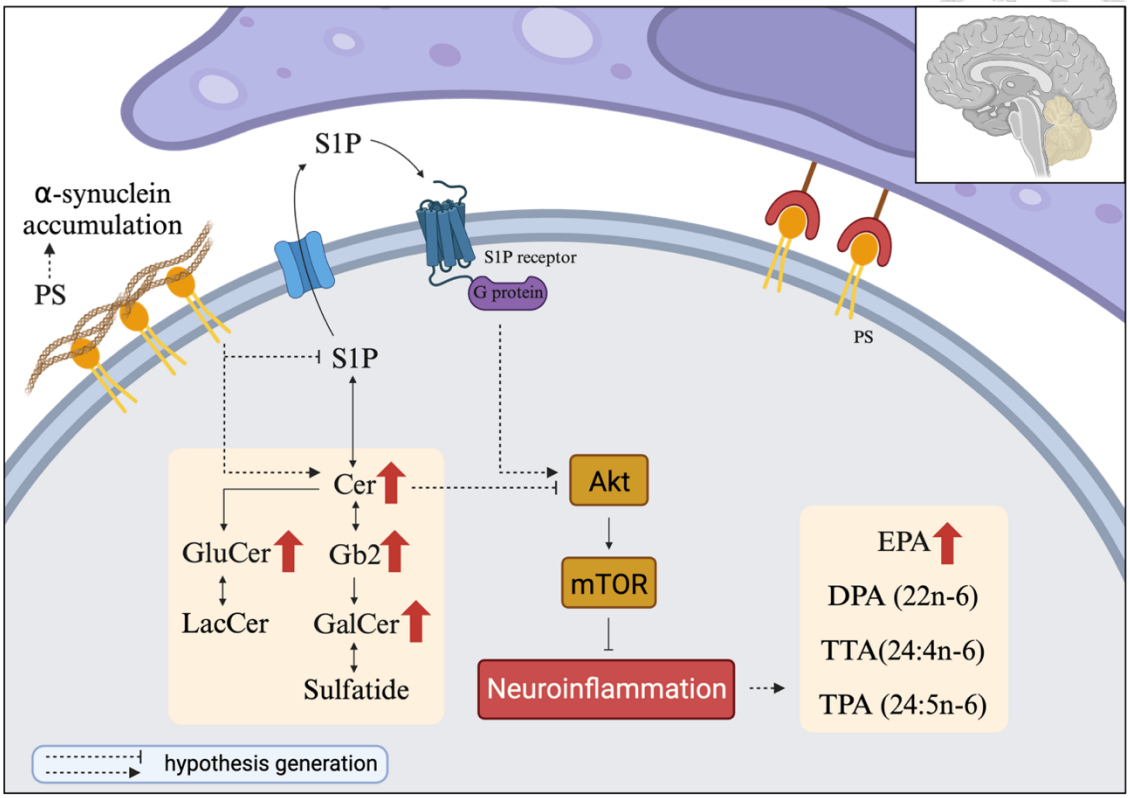

Figure 4.4 The alteration of sphingolipid, unsaturated fatty acids, and phosphatidylserine in the vermis of cerebellum. The arrows indicate an absolute ln-fold change > 1.5.

doi:10.6342/NTU202304442

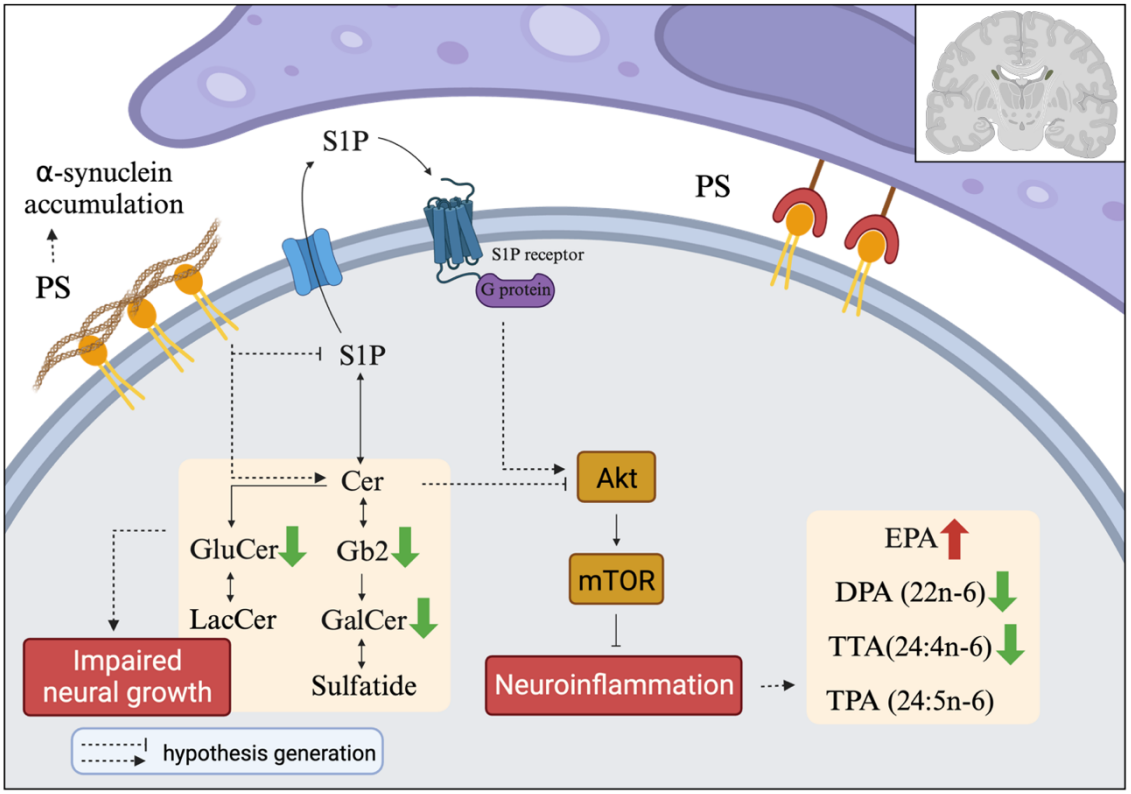

Figure 4.5 The alteration of sphingolipid, unsaturated fatty acids, and phosphatidylserine in the putamen. The arrows indicate an absolute ln-fold change > 1.5.

doi:10.6342/NTU202304442

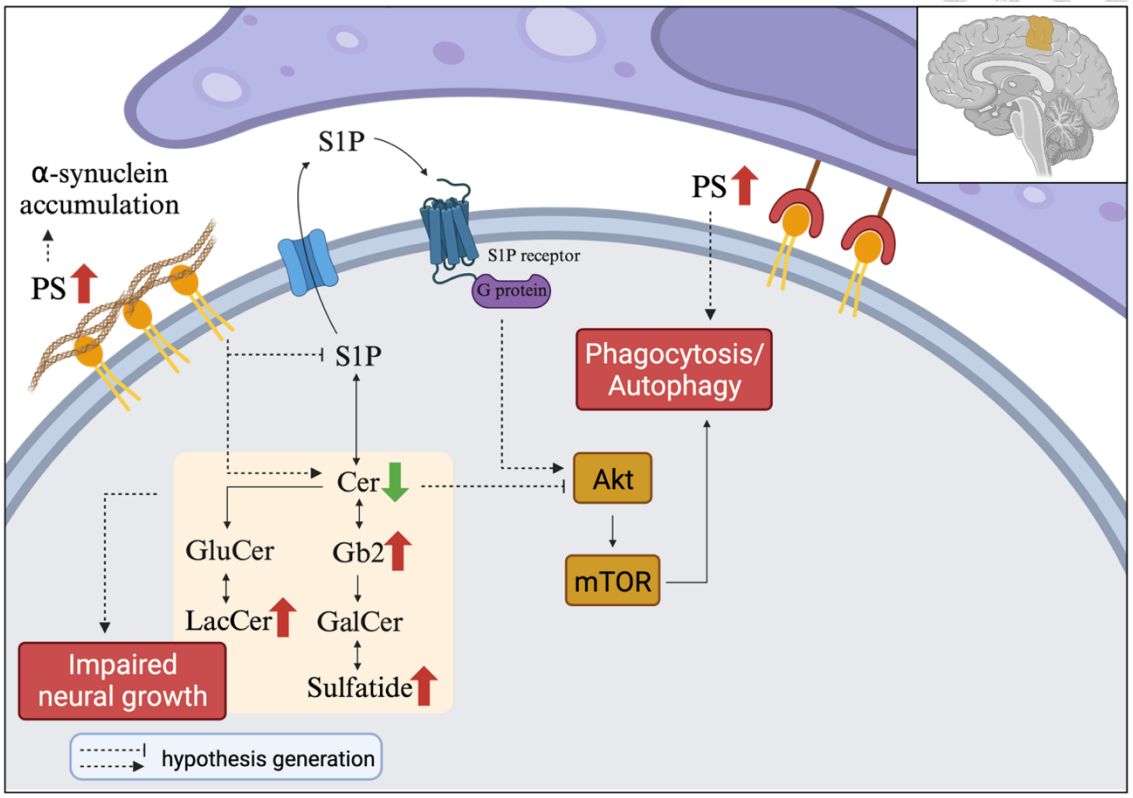

Figure 4.6 The alteration of sphingolipid, unsaturated fatty acids, and phosphatidylserine in the motor cortex. The arrows indicate an absolute ln-fold change > 1.5.

Overall, according to the initial statistical analysis, we identified elevated levels of EPA, PS, and sulfatide species in the brains of MSA patients regardless of the brain regions. As shown in Figure 4.7, elevated sulfatides induce impaired neural growth by inhibiting oligodendrocyte outgrowth[64], and this effect mainly occurred in several cerebral cortexes. Elevated PS species trigger the downstream phagocytosis in the apoptotic process[65]. Moreover, PS enhances the aggregation of α-synuclein by directly binding to its α-helix domain, impairing the membrane permeability of neural cells and causing neuroinflammation.[16] In our results, these events also mainly affected the cerebral cortex. Elevated EPA has been considered a lipid biomarker for MSA. Our results showed an overall elevation of EPA in most brain regions, especially in the brain regions

doi:10.6342/NTU202304442

of the basal ganglia and cerebellum, which has been considered the compensatory effect for neuroinflammation induced by the accumulation of α-synuclein. These lipid alterations are consistent with the results of previous studies regarding MSA lipid expression.[21][25][26] We also identified ceramide as a significantly altered lipid in the cerebellum that has not been reported before, and the elevation can also induce neuroinflammation and neuronal death.[63]

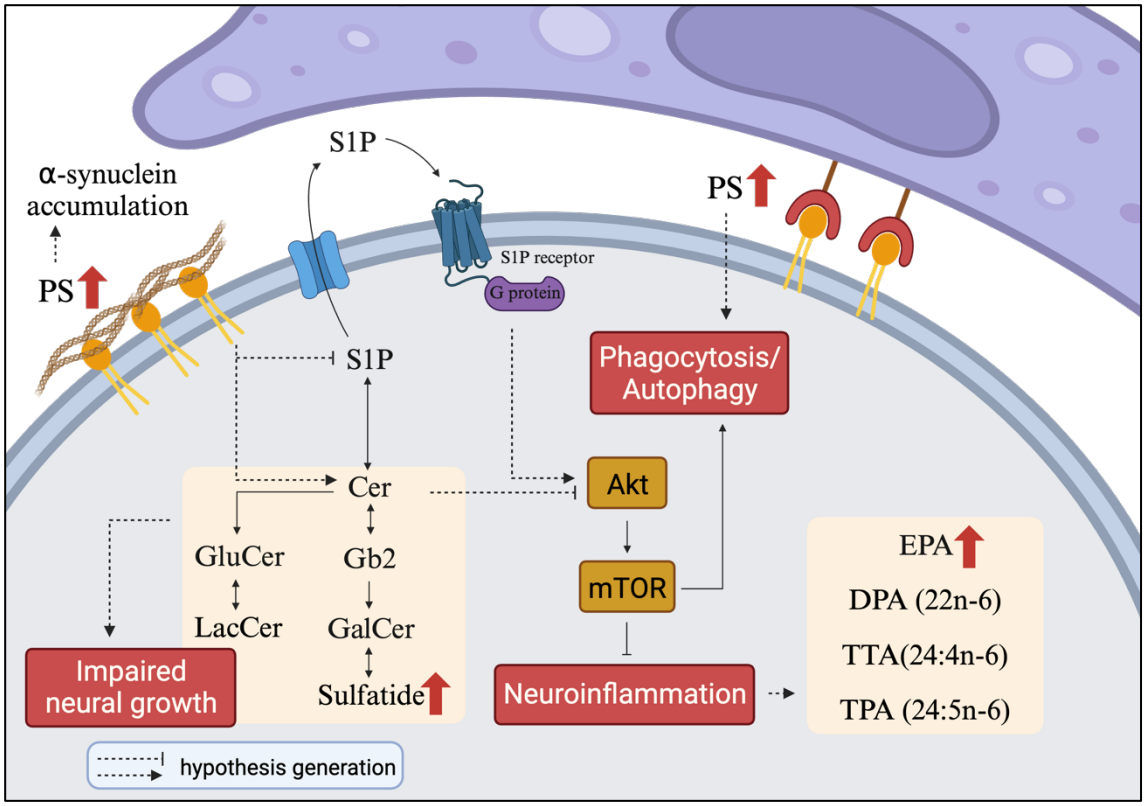

Figure 4.7 The alteration of sphingolipid, unsaturated fatty acids, and phosphatidylserine in the MSA group compared to that of the healthy control regardless of the brain regions. The arrows indicate the initial statistical results with an adjusted p value under 0.05.

doi:10.6342/NTU202304442

To our knowledge, there have been few metabolomic-based studies on metabolite alterations of the cerebellum and the basal ganglia of MSA patients. These results could represent pioneering findings on lipid disturbances in these brain regions of MSA patients. Although some other brain regions, such as motor cortex and amygdala[25][26], have been studied in previous works, the sample sizes were also limited (eight and eight, respectively). The previous inferences in Section 4.1.4 about how lipid alterations affect each brain region in MSA disease progression were only based on the tentative lipid changes and the literature review. The actual lipid disturbances in different brain regions caused by MSA still need more tissue samples and mass spectrometry data to verify the key lipids that can act as the disease biomarkers. However, this study can serve as introductory research to screen for possible disease-related metabolite alterations for understanding the detailed disease mechanisms and their effects to different regions of the tissues and organs.

doi:10.6342/NTU202304442

4.1.5 The Distribution of α-Synuclein is Spatially Correlated with the Lipid Pattern Detected by MSI

Since the abnormal accumulation of α-synuclein and the alteration of lipids can induce neural degeneration and neuroinflammation, we further demonstrated the spatial correlation between α-synuclein and lipids by aligning α-synuclein staining and mass spectrometry images. Figure 3.10 and Table 3.3 show that ceramide, cerebroside, sulfatide, and phosphatidylserine are spatially correlated with α-synuclein accumulation. In Section 4.1.2, ceramides and cerebrosides are described as important lipids for neuronal growth. Sulfatide species maintain myelin stability, while the overexpression of sulfatide can inhibit oligodendrocyte differentiation. Our results showed that ceramide d36:1, d38:1, and d42:2, glucosylceramide d36:1, galactosylceramide d36:1, glucosylceramide d42:2, galactosylceramide d42:2, galabiosylceramide d36:2, and lactosylceramide d36:2, sulfatide d36:1, d36:2, d42:2 and d44:2 are spatially correlated with α-synuclein. The expression of these lipids was significantly altered in the brains of the MSA group. Expression is spatially correlated with α-synuclein accumulation, indicating that α-synuclein accumulation can directly affect the expression and distribution of these lipids, inducing downstream neural loss and inflammation. Phosphatidylserine acts as a signal for programmed cell death. Although our results showed little consistency in the alteration trends among different PS species, we found that PS 40:3, PS 42:4, and PS 42:5 are elevated in some cerebral cortices, such as the orbitofrontal cortex, motor cortex, and sensory cortex. Moreover, according to the data shown in Table 3.3, there is a spatial correlation between these PS species and α-synuclein accumulation, indicating that the accumulation has triggered events for programmed cell death in these regions and has led to subsequent neural loss. Although the differential test

doi:10.6342/NTU202304442

and pathway analysis showed that the unsaturated fatty acids, especially EPA, were significantly elevated in the MSA brain, they showed no spatial correlation with α-synuclein accumulation, and their distribution is not limited to a specific area in the brain. This suggests that the elevation of EPA may be a physiological consequence for regulating neuroinflammation rather than directly affecting or being affected by α-synuclein.

This is the first study that explore the spatial distribution and correlation of the protein biomarker, α-synuclein, and other potential lipid biomarkers in MSA patient brain regions. However, we still need more tissue samples to investigate the detailed effects and disease mechanisms of the spatial correlation of protein and lipid biomarkers in each brain region.

4.2 Limitations

In this study, there was only one human brain tissue sample in MSA group and in the control group. We used 12 brain regions as 12 samples within each group. As different brain regions carry out different physiological functions, they can present other traits in the lipid profile. Hence, there was a relatively sizeable within-group variation in our statistical analysis. Although we could identify significant alterations in some previously studied lipids, we cannot rule out the possibility that the difference might be caused by another physiological or pathological status between the two individuals. Moreover, for the alteration of lipid expression in different brain regions, the explanatory power could be limited, as there was only one sample from each group for each brain region.

Second, for MSI data, the annotation was only based on the monoisotopic molecular weight, so one m/z value can be mapped to various candidate molecules. Although we ruled out some candidates not involved in human biochemical pathways, there were still

doi:10.6342/NTU202304442

some m/z values that could represent multiple candidate molecules. For example, m/z 742.54 represents the molecular formula of C41H78NO8P, which can be formed as PC 33:2 or PE 26:2, and these two lipid species can also be included as various lipid isomers with different combinations of fatty acyl chains. Therefore, it was challenging to distinguish between the PC and PE species only by MSI data.

We did not identify some reported lipid alterations in this study. For example, α-synuclein has been reported to decrease sphingosine-1-phosphate in plasma[23] and sphingomyelin[25] in the motor cortex, leading to impaired neuronal growth. Studies have indicated that overexpression of α-synuclein can inhibit the synthesis of sphingosine-1-phosphate in PD patients, resulting in the decrease level of sphingosine-1-phosphate and increased level of its material, ceramide. Additionally, ceramide and sphingosine-1-phosphate exerts antagonism effects in the regulation of Akt/mTOR signaling pathway.[73] As the pathway both negatively regulates inflammation and positively regulates neural death and apoptosis, the balance between ceramide and sphingosine-1-phosphate level can be important factor to determine the dominant pathological events in patients' brain. Although we have identified varying alterations of ceramide level in different brain regions, the mass signal of sphingosine-1-phosphate was not detected in this study. Additionally, elevated levels of PC and PE have been found in the amygdala in the MSA patients[26]. The elevation of PC and PE can also enhance the aggregation of α-synuclein and affect cell membrane stability. Despite identifying elevated levels of certain PC and PE species in most brain regions, the results displayed inconsistencies across different species with varying carbon chain lengths and degrees of unsaturation. Furthermore, EPA and docosahexaenoic acid (DHA) are both well-known anti-inflammatory ω-3 unsaturated fatty acids. Previous studies have indicated that EPA was elevated in CSF of the MSA patients[21], while the supplementation of DHA in

doi:10.6342/NTU202304442

oligodendroglial cell membrane can enhance the aggregation of α-synuclein.[74] In our study, EPA and DHA were detected in most brain regions. EPA was elevated in most brain regions of the MSA patients, while no significant alterations of DHA was found between the MSA and control groups.

doi:10.6342/NTU202304442

Chapter 5 Conclusions

This study analyzed the 12 brain regions of postmortem brains from one MSA patient and one HC by DESI-MSI and IHC. Through DESI-MSI, we acquired the average signal intensity and spatial distribution of lipids in the 12 brain regions. We found that most metabolites with significant alterations belong to the class of sphingolipids, glycerophospholipids, and unsaturated fatty acids. Sphingolipids, such as ceramides, cerebrosides, and sulfatides have been found to regulate neuroinflammation neuronal growth and myelin stability. Glycerophospholipids maintain the stability of neural cell membranes and regulate the programmed cell cycle. Unsaturated fatty acids are important lipids for neuroinflammation. We investigated lipid disturbances in different brain regions and found that varying lipid disturbances indicated different pathological statuses of the different brain regions. IHC staining was used to visualize the distribution of α-synuclein accumulation. We found that the distribution of α-synuclein accumulation was spatially correlated with that of some ceramide, cerebroside, sulfatide, and phosphatidylserine species. These results indicated that the abnormal accumulation of α-synuclein is positively related to the distribution of the sphingolipids and glycerophospholipids. However, no spatial correlation between α-synuclein accumulation and unsaturated fatty acids was found, indicating that the abnormal accumulation of α-synuclein and the alteration of unsaturated fatty acids has no direct mutual effect. Finally, although we did not identify a few reported lipid alterations in the MSA patients, we demonstrated that DESI-MSI is effective enough to detect some lipid alterations and their distributions in MSA patients. This approach allows more detailed research on the disease mechanism induced by these lipids in the different brain regions of MSA patients.

doi:10.6342/NTU202304442

REFERENCE

[1] Buchberger AR, DeLaney K, Johnson J, Li L. Mass Spectrometry Imaging: A Review of Emerging Advancements and Future Insights. *Anal Chem*. 2018 Jan 2;90(1):240-265.

[2] Erika R. Amstalden van Hove, Donald F. Smith, Ron M.A. Heeren. A concise review of mass spectrometry imaging. *Journal of Chromatography A*, Volume 1217, Issue 25, 2010, Pages 3946-3954.

[3] Bernhard Spengler. Mass Spectrometry Imaging of Biomolecular Information. *Anal. Chem*. 2015, 87, 1, 64–82.

[4] Xin Ma, Recent Advances in Mass Spectrometry-Based Structural Elucidation Techniques, *Molecules*, 10.3390/molecules27196466, 27, 19, (6466), (2022).

[5] Randall EC, Zadra G, Chetta P, Lopez BGC, Syamala S, Basu SS, Agar JN, Loda M, Tempany CM, Fennessy FM, Agar NYR. Molecular Characterization of Prostate Cancer with Associated Gleason Score Using Mass Spectrometry Imaging. *Mol Cancer Res*. 2019 May;17(5):1155-1165.

[6] Tu A, Said N, Muddiman DC. Spatially resolved metabolomic characterization of muscle invasive bladder cancer by mass spectrometry imaging. *Metabolomics*. 2021 Jul 21;17(8):70.

[7] Aramaki S, Tsuge S, Islam A, Eto F, Sakamoto T, Oyama S, *et al*. (2023) Lipidomics-based tissue heterogeneity in specimens of luminal breast cancer revealed by clustering analysis of mass spectrometry imaging: A preliminary study. *PLoS ONE* 18(5): e0283155.

[8] Zhang G, Zhang J, DeHoog RJ, Pennathur S, Anderton CR, Venkatachalam MA, Alexandrov T, Eberlin LS, Sharma K. DESI-MSI and METASPACE indicate lipid

doi:10.6342/NTU202304442

abnormalities and altered mitochondrial membrane components in diabetic renal proximal tubules. *Metabolomics*. 2020 Jan 10;16(1):11.

[9] Maccarrone G, Nischwitz S, Deininger SO, Hornung J, König FB, Stadelmann C, Turck CW, Weber F. MALDI imaging mass spectrometry analysis-A new approach for protein mapping in multiple sclerosis brain lesions. *J Chromatogr B Analyt Technol Biomed Life Sci*. 2017 Mar 15;1047:131-140.

[10] Hare DJ, Raven EP, Roberts BR, Bogeski M, Portbury SD, McLean CA, Masters CL, Connor JR, Bush AI, Crouch PJ, Doble PA. Laser ablation-inductively coupled plasma-mass spectrometry imaging of white and gray matter iron distribution in Alzheimer's disease frontal cortex. *Neuroimage*. 2016 Aug 15;137:124-131.

[11] Sandra Schulz, Michael Becker, M. Reid Groseclose, Simone Schadt, Carsten Hopf. Advanced MALDI mass spectrometry imaging in pharmaceutical research and drug development, *Current Opinion in Biotechnology*, Volume 55, 2019, Pages 51-59.

[12] Bonnel D, Legouffe R, Eriksson AH, Mortensen RW, Pamelard F, Stauber J, Nielsen KT. MALDI imaging facilitates new topical drug development by determining quantitative skin distribution profiles. *Anal Bioanal Chem*. 2018 Apr;410(11):2815-2828.

[13] Landry Blanc, Anne Lenaerts, Véronique Dartois, and Brendan Prideaux. Visualization of Mycobacterial Biomarkers and Tuberculosis Drugs in Infected Tissue by MALDI-MS Imaging. *Anal. Chem*. 2018, 90, 10, 6275–6282

[14] Anna Nilsson, Richard J. A. Goodwin, John G. Swales, Richard Gallagher, Harish Shankaran, Abhishek Sathe, Selvi Pradeepan, Aixiang Xue, Natalie Keirstead, Jennifer C. Sasaki, Per E. Andren, and Anshul Gupta. Investigating Nephrotoxicity of Polymyxin Derivatives by Mapping Renal Distribution Using Mass Spectrometry Imaging. *Chem. Res. Toxicol*. 2015, 28, 9, 1823–1830.

doi:10.6342/NTU202304442

[15] Gregor K Wenning, Carlo Colosimo, Felix Geser, Werner Poewe. Multiple system atrophy, *The Lancet Neurology*, Volume 3, Issue 2, 2004, Pages 93-103.

[16] Wenning, G.K., Stankovic, I., Vignatelli, L., Fanciulli, A., Calandra-Buonaura, G., Seppi, K., Palma, J., Meissner, W.G., Krismer, F., Berg, D., *et al.* (2022), The Movement Disorder Society Criteria for the Diagnosis of Multiple System Atrophy. *Mov Disord*, 37: 1131-1148.

[17] Segrest JP, Jones MK, De Loof H, Brouillette CG, Venkatachalapathi YV, Anantharamaiah GM. The amphipathic helix in the exchangeable apolipoproteins: a review of secondary structure and function. *J Lipid Res*. 1992 Feb;33(2):141-66.

[18] Lv Z, Hashemi M, Banerjee S, Zagorski K, Rochet JC, Lyubchenko YL. Assembly of α-synuclein aggregates on phospholipid bilayers. *Biochim Biophys Acta Proteins Proteom*. 2019 Sep;1867(9):802-812.

[19] Lee HJ, Khoshaghideh F, Patel S, Lee SJ. Clearance of alpha-synuclein oligomeric intermediates via the lysosomal degradation pathway. *J Neurosci*. 2004 Feb 25;24(8):1888-96.

[20] Heather McCann, Claire H. Stevens, Heidi Cartwright, Glenda M. Halliday. α-Synucleinopathy phenotypes. *Parkinsonism & Related Disorders*, Volume 20, Supplement 1, 2014, Pages S62-S67.

[21] Lee, P.H.; Lee, G.; Paik, M.J. Polyunsaturated fatty acid levels in the cerebrospinal fluid of patients with Parkinson's disease and multiple system atrophy. *Mov Disord*. 2008, 23, 309–310.

[22] Akio Mori, Kei-Ichi Ishikawa, Shinji Saiki, Taku Hatano, Yutaka Oji, Ayami Okuzumi, Motoki Fujimaki, Takahiro Koinuma, Shin-Ichi Ueno, Yoko Imamichi, Nobutaka Hattori. Plasma metabolite biomarkers for multiple system atrophy and progressive supranuclear palsy. *PLoS ONE*, 2019, 14(9): e0223113.

doi:10.6342/NTU202304442

[23] Oizumi H, *et al*. Plasma sphingolipid abnormalities in neurodegenerative diseases. *PLoS ONE*, 2022, 17(12): e0279315.

[24] Motyl, J.A., Strosznajder, J.B., Wencel, A., Strosznajder, R.P. Recent Insights into the Interplay of Alpha-Synuclein and Sphingolipid Signaling in Parkinson's Disease. *Int. J. Mol. Sci.* 2021, *22*, 6277.

[25] Don, A.S., Hsiao, JH.T., Bleasel, J.M. *et al.* Altered lipid levels provide evidence for myelin dysfunction in multiple system atrophy. *Acta Neuropathologica Communications*, 2014, 2:150.

[26] Fu, Y., He, Y., Phan, K. *et al.* Increased unsaturated lipids underlie lipid peroxidation in synucleinopathy brain. *Acta Neuropathologica Communications* (2022) 10:165.

[27] Calder, P. N-3 Fatty acids, inflammation and immunity: new mechanisms to explain old actions. *Proceedings of the Nutrition Society*, 2013, 72(3), 326-336.

[28] Kalogeropoulos N, Panagiotakos DB, Pitsavos C, Chrysohoou C, Rousinou G, Toutouza M, Stefanadis C. Unsaturated fatty acids are inversely associated and n-6/n-3 ratios are positively related to inflammation and coagulation markers in plasma of apparently healthy adults. *Clin Chim Acta*. 2010 Apr 2;411(7-8):584-91.

[29] Masahiro Maruoka, Jun Suzuki. Regulation of phospholipid dynamics in brain, *Neuroscience Research*, Volume 167, 2021, Pages 30-37.

[30] Olsen Anne S. B. and Fergeman Nils J. Sphingolipids: membrane microdomains in brain development, function and neurological diseases. *Open Biol*, 2017, 7:170069.

[31] Fellner L, Wenning GK, Stefanova N. Models of multiple system atrophy. *Curr Top Behav Neurosci*. 2015, 22:369-93.

[32] Volkow ND, Wang GJ, Newcorn JH, Kollins SH, Wigal TL, Telang F, Fowler JS, Goldstein RZ, Klein N, Logan J, Wong C, Swanson JM. Motivation deficit in

doi:10.6342/NTU202304442

ADHD is associated with dysfunction of the dopamine reward pathway. *Mol Psychiatry*. 2011 Nov;16(11):1147-54.

[33] Goldstein, D.S.; Holmes, C.; Sharabi, Y. Cerebrospinal fluid biomarkers of central catecholamine deficiency in Parkinson's disease and other synucleinopathies. *Brain* 2012, 135, 1900–1913.

[34] Abdo WF, De Jong D, Hendriks JC, Horstink MW, Kremer BP, Bloem BR, Verbeek MM. Cerebrospinal fluid analysis differentiates multiple system atrophy from Parkinson's disease. *Mov Disord*. 2004 May;19(5):571-9.

[35] Chen D, Wan L, Chen Z, Yuan X, Liu M, Tang Z, Fu Y, Zhu S, Zhang X, Qiu R, Tang B, Jiang H. Serum vitamin levels in multiple system atrophy: A case-control study. *Front Aging Neurosci.* 2023 Jan 5;14:1105019.

[36] Moschou PN, Roubelakis-Angelakis KA. Polyamines and programmed cell death. *J Exp Bot.* 2014 Mar;65(5):1285-96.

[37] Paik MJ, Ahn YH, Lee PH, Kang H, Park CB, Choi S, Lee G. Polyamine patterns in the cerebrospinal fluid of patients with Parkinson's disease and multiple system atrophy. *Clin Chim Acta*. 2010 Oct 9;411(19-20):1532-5.

[38] Kuiper MA, Teerlink T, Visser JJ, Bergmans PL, Scheltens P, Wolters EC. L-glutamate, L-arginine and L-citrulline levels in cerebrospinal fluid of Parkinson's disease, multiple system atrophy, and Alzheimer's disease patients. *J Neural Transm (Vienna)*. 2000;107(2):183-9.

[39] Kuiper MA, Visser JJ, Bergmans PL, Scheltens P, Wolters EC. Decreased cerebrospinal fluid nitrate levels in Parkinson's disease, Alzheimer's disease and multiple system atrophy patients. *J Neurol Sci*. 1994 Jan;121(1):46-9.

[40] Compta Y, Giraldo DM, Muñoz E, Antonelli F, Fernández M, Bravo P, Soto M, Cámara A, Torres F, Martí MJ; Catalan MSA Registry (CMSAR). Cerebrospinal

doi:10.6342/NTU202304442

fluid levels of coenzyme Q10 are reduced in multiple system atrophy. *Parkinsonism Relat Disord*. 2018 Jan;46:16-23.

[41] Richard J.A. Goodwin, Sample preparation for mass spectrometry imaging: Small mistakes can lead to big consequences, *Journal of Proteomics*, Volume 75 Issue 16, 2012, Pages 4893-4911.

[42] Rueden, C.T., Schindelin, J., Hiner, M.C. *et al.* ImageJ2: ImageJ for the next generation of scientific image data. *BMC Bioinformatics* 18, 529 (2017).

[43] Palmer, A., Phapale, P., Chernyavsky, I. *et al*. FDR-controlled metabolite annotation for high-resolution imaging mass spectrometry. *Nat Methods* 14, 57–60 (2017).

[44] David S Wishart and others, HMDB 5.0: the Human Metabolome Database for 2022, *Nucleic Acids Research*, Volume 50, Issue D1, 7 January 2022, Pages D622–D631.

[45] Kind, T., Fiehn, O. Metabolomic database annotations via query of elemental compositions: Mass accuracy is insufficient even at less than 1 ppm. *BMC Bioinformatics* 7, 234 (2006).

[46] Theodore Alexandrov, Andreas Bartels, Testing for presence of known and unknown molecules in imaging mass spectrometry, *Bioinformatics*, Volume 29, Issue 18, 15 September 2013, Pages 2335–2342.

[47] Elias JE, Gygi SP. Target-decoy search strategy for mass spectrometry-based proteomics. *Methods Mol Biol*. 2010; 604:55-71.

[48] Pang, Z., Zhou, G., Ewald, J. *et al*. Using MetaboAnalyst 5.0 for LC–HRMS spectra processing, multi-omics integration and covariate adjustment of global metabolomics data. *Nat Protoc* 17, 1735–1761 (2022).

[49] Wei R, Wang J, Su M, Jia E, Chen S, Chen T, Ni Y. Missing Value Imputation

doi:10.6342/NTU202304442

Approach for Mass Spectrometry-based Metabolomics Data. *Sci Rep*. 2018 Jan 12;8(1):663.

[50] Kanehisa M, Furumichi M, Tanabe M, Sato Y, Morishima K. KEGG: new perspectives on genomes, pathways, diseases and drugs. *Nucleic Acids Res*. 2017 Jan 4; 45(D1):D353-D361.

[51] Kim S, Cheng T, He S, Thiessen PA, Li Q, Gindulyte A, Bolton EE. PubChem Protein, Gene, Pathway, and Taxonomy Data Collections: Bridging Biology and Chemistry through Target-Centric Views of PubChem Data. *J Mol Biol*. 2022 Feb 25:167514.

[52] Benjamin Balluff, Ron M.A. Heeren, Alan M. Race. An overview of image registration for aligning mass spectrometry imaging with clinically relevant imaging modalities, *Journal of Mass Spectrometry and Advances in the Clinical Lab*, Volume 23, 2022, Pages 26-38.

[53] Bo-Jhang Lin, Tien-Chueh Kuo, Hsin-Hsiang Chung, Ying-Chen Huang, Ming-Yang Wang, Cheng-Chih Hsu, Po-Yang Yao, and Yufeng Jane Tseng. MSIr: Automatic Registration Service for Mass Spectrometry Imaging and Histology. *Analytical Chemistry*, 2023 95 (6), 3317-3324

[54] I. Klinkert, K. Chughtai, S.R. Ellis, and R.M.A. Heeren. Methods for full resolution data exploration and visualization for large 2D and 3D mass spectrometry imaging datasets, *International Journal of Mass Spectrometry*, 2014. 362: p. 40-47.

[55] S. Klein, M. Staring, K. Murphy, M.A. Viergever, J.P.W. Pluim, "elastix: a toolbox for intensity based medical image registration," *IEEE Transactions on Medical Imaging*, vol. 29, no. 1, pp. 196 - 205, January 2010.

[56] Prasad, M., Postma, G., Franceschi, P. *et al.* Evaluation and comparison of unsupervised methods for extracting spatial patterns from mass spectrometry

doi:10.6342/NTU202304442

imaging data (MSI). *Sci Rep* 12, 15687 (2022).

[57] Shutaywi M, Kachouie NN. Silhouette Analysis for Performance Evaluation in Machine Learning with Applications to Clustering. *Entropy (Basel)*. 2021 Jun 16;23(6):759.

[58] Mota-Martorell, N., Andrés-Benito, P., Martín-Gari, M. *et al.* Selective brain regional changes in lipid profile with human aging. *GeroScience* **44**, 763–783 (2022).

[59] Hannun YA, Obeid LM. The Ceramide-centric Universe of Lipid-mediated Cell Regulation: Stress Encounters of the Lipid Kind. *Journal of Biological Chemistry,* Volume 277, Issue 29, 25847 – 25850.

[60] Hetz CA, Hunn M, Rojas P, Torres V, Leyton L, Quest AF. Caspase-dependent initiation of apoptosis and necrosis by the Fas receptor in lymphoid cells: onset of necrosis is associated with delayed ceramide increase. *J Cell Sci*. 2002 Dec 1;115(Pt 23):4671-83.

[61] Snider AJ, Orr Gandy KA, Obeid LM. Sphingosine kinase: Role in regulation of bioactive sphingolipid mediators in inflammation. *Biochimie*. 2010 Jun;92(6):707-15.

[62] Marcus J, Honigbaum S, Shroff S, Honke K, Rosenbluth J, Dupree JL. Sulfatide is essential for the maintenance of CNS myelin and axon structure. *Glia*. 2006 Mar;53(4):372-81.

[63] Mencarelli C, Martinez-Martinez P. Ceramide function in the brain: when a slight tilt is enough. Cell Mol Life Sci. 2013 Jan;70(2):181-203.

[64] Winzeler AM, Mandemakers WJ, Sun MZ, Stafford M, Phillips CT, Barres BA. The lipid sulfatide is a novel myelin-associated inhibitor of CNS axon outgrowth. *J Neurosci*. 2011 Apr 27;31(17):6481-92.

doi:10.6342/NTU202304442

[65] Erekat, N. S. (2022). Apoptosis and its therapeutic implications in neurodegenerative diseases. *Clinical Anatomy*, 35(1), 65-78.

[66] Hirahara Y, Bansal R, Honke K, Ikenaka K, Wada Y. Sulfatide is a negative regulator of oligodendrocyte differentiation: development in sulfatide-null mice. *Glia*. 2004 Feb;45(3):269-77.

[67] Xiao, S., Finkielstein, C.V., Capelluto, D.G.S. (2013). The Enigmatic Role of Sulfatides: New Insights into Cellular Functions and Mechanisms of Protein Recognition. In: Capelluto, D. (eds) Lipid-mediated Protein Signaling. *Advances in Experimental Medicine and Biology*, vol 991.

[68] Calder PC. Omega-3 fatty acids and inflammatory processes. *Nutrients*. 2010 Mar;2(3):355-374.

[69] Innes JK, Calder PC. Omega-6 fatty acids and inflammation. *Prostaglandins Leukot Essent Fatty Acids*. 2018 May; 132:41-48.

[70] Poewe, W., Stankovic, I., Halliday, G. *et al.* Multiple system atrophy. *Nat Rev Dis Primers* 8, 56 (2022).

[71] Bikman BT, Summers SA. Ceramides as modulators of cellular and whole-body metabolism. *J Clin Invest.* 2011 Nov;121(11):4222-30.

[72] Chakravarthy, V.S., Joseph, D. & Bapi, R.S. What do the basal ganglia do? A modeling perspective. *Biol Cybern* 103, 237–253 (2010).

[73] Czubowicz K, Jęśko H, Wencel P, Lukiw WJ, Strosznajder RP. The Role of Ceramide and Sphingosine-1-Phosphate in Alzheimer's Disease and Other Neurodegenerative Disorders. *Mol Neurobiol.* 2019 Aug;56(8):5436-5455.

[74] Riedel M, Goldbaum O, Wille M, Richter-Landsberg C. Membrane lipid modification by docosahexaenoic acid (DHA) promotes the formation of α-synuclein inclusion bodies immunopositive for SUMO-1 in oligodendroglial cells

doi:10.6342/NTU202304442

after oxidative stress. *J Mol Neurosci.* 2011 Mar;43(3):290-302.

doi:10.6342/NTU202304442